EDHA for Energy Production, Storage and Conversion Devices

Kelder, Erik; Marijnissen, Jan; Karuga, Susan

DOI
10.1016/j.jaerosci.2018.04.011

Publication date
2018

Document Version
Accepted author manuscript

Published in
Journal of Aerosol Science

Citation (APA)
Kelder, E., Marijnissen, J., & Karuga, S. (2018). EDHA for Energy Production, Storage and Conversion Devices. *Journal of Aerosol Science*, *25*(11), Article AS5279. https://doi.org/10.1016/j.jaerosci.2018.04.011

EDHA for Energy Production, Storage and Conversion Devices

E.M. Kelder, J.C.M. Marijnissen, S. Waiyego Karuga

www.elsevier.com/locate/jaerosci

PII: S0021-8502(17)30432-9
DOI: https://doi.org/10.1016/j.jaerosci.2018.04.011
Reference: AS5279

To appear in: *Journal of Aerosol Science*

Received date: 31 October 2017
Revised date: 30 April 2018
Accepted date: 30 April 2018

Cite this article as: E.M. Kelder, J.C.M. Marijnissen and S. Waiyego Karuga, EDHA for Energy Production, Storage and Conversion Devices, *Journal of Aerosol Science,* https://doi.org/10.1016/j.jaerosci.2018.04.011

EDHA for Energy Production, Storage and Conversion Devices

E.M. Kelder[1*], J.C.M. Marijnissen[2], S. Waiyego Karuga[2]

[1]Delft University of Technology, Faculty of Applied Sciences, Department of radiation Science and Technology, Mekelweg 15, 2629 BJ Delft, The Netherlands

[2]University of Nairobi, Nuclear Science and Technology, University Way, Nairobi, Kenia

[*]corresponding author.

Abstract

Electrohydrodynamic atomization (EHDA) or electrospraying stands out in thin film deposition because of its unique ability to form charged droplets, initiating higher deposition efficiencies in electrostatic spray deposition. Considering that the quality of a thin film depends on the particle sizes, their monodispersity and uniform distribution on the surface, electrospray is a powerful tool in materials synthesis. Therefore, this review looks at different areas where this novel technique has been used to improve on the overall performance of materials for energy devices, such as solar cells, photoelectrochemical cells, rechargeable batteries and beyond, capacitors, and (O)LEDs, including quantum dots.

List of abbreviations used

AlN, Aluminium Nitride; AN, Acetonitrile; CB, Chlorobenzene; CIGS, Cu-In-Ga-Se; CIGSSe, $Cu(InGa)(SSe)_2$; CIS, Copper Indium Sulfides/Selenides; CNT, Carbon Nanotube; CN-PPV, poly[2,5-di(hexyloxy)cyanoterephthalylidene]; CV, Cyclic Voltammetry; CZTS, Copper-Zinc-Tin-Sulfide; CZTSe, Copper-Zinc-Tin-Selenide; CZTSSe, Copper-Zinc-Tin-Sulfide/selenide; DCB, Dihlorobenzene; DCE, 1,2-dichloroethane; EC, Electrochemical Capacitor; EHDA, ElectroHydroDynamic Atomization (EHDA; EL, ElectroLuminescence; EML, Emissive Layer; ESAVD, ElectroSpray Assisted Vapour Deposition; ESD, Electrostatic Spray Deposition; FF, Fill Factor; FTO, Fluorinated Tin Oxide; GNP, Graphene Nano-Platelet; GO, Graphene Oxide; IR, InfraRed; $Ir(mppy)_3$, tris(2-(4-tolyl)phenylpyridine)iridium; ITO, Indium Tin Oxide; LED, Light Emitting Diode; LIB, Lithium Ion Battery; Li-S, Lithium Sulfur; MEH-PPV, poly[2-methoxy-5-(2ethylhexyloxy)-1,4-phenylenevinylene; MPBL, Multifunctional Polysulfide Blocking Layer; MWNT, Multi-Walled Carbon Tube; NPCS-S, Hybrid Sulfur and Nitrogen-Doped Porous Carbon Sheet (NPCS); NVP, Sodium Vanadium Phosphate ($Na_3V_2(PO_4)_3$; OLED, Organic Light Emitting Diode; OPV, Organics PhotoVoltaics; OTFT, Organic Thin Flm Transistors; PAN, Polyacrylnitrile; PBD, 2-(4-biphenylyl)-5-(4-tert-butylphenyl)-1,3,4-oxadiazole; PCE, Power Connversion Efficiency; PCNF, Porous Carbon-NanoFiber; PEC, PhotoElectrochemical Cell; (PE)CVD, Plasma-Enhanced Chemical Vapour Deposition; PEDOT:PSS, poly(3,4-ethylenedioxythiophene): polystyrene sulfonate; PLED, Polymer Light-Emitting Diode; PSC, Perovskite Based Solar Cells; PVK, Poly(N-vinyl carbazole; rGO, reduced Graphene Oxide; RHE, Reversible Hydrogen Electrode; SEM, Scanning Electrochemical Microscopy; TCO, Transparent Conductive Oxide; TPD, N,N'diphenyl-N,N'-bis(3-methylphenyl)-[1,1-biphenyl]-4,4'-diamine; QD, Quantum Dot; XRD, X-Ray Diffraction

Keywords: EHDA; Electrospraying; ESD; Li-ion batteries, Solar cells

1 Introduction

Electrohydrodynamic atomization (EHDA) or electrospraying stands out in thin film deposition because of its unique ability to form charged droplets hence higher deposition efficiency, i.e. electrostatic spray deposition (ESD), which term will be used further throughout this chapter. It involves disintegration of a liquid into airborne droplets by applying an electric field which causes shear stress on the liquid surface leading to elongation of a jet that breaks up into small charged droplets. Due to the mutual Coulomb repulsion among the droplets, there is self-dispersion on the substrate hence no agglomeration resulting in uniform deposition on inhomogeneous surfaces (Lee et al., 2007; Yoon et al., 2003; Cao et al., 2002; Nishizawa et al., 1998; Chen et al., 1995; van Zomeren, 1994). For instance, with an aim of synthesizing Co_3O_4

thin films on a glass substrate, Abbas et al. (2017) confirmed the effect of an electric field during deposition. From their results, the film deposited with no electric field showed flaws like crystal flakes, pin holes and many cracks on the surface while the film grown under an electric field appeared smoother and more homogeneous with well-formed grains. With these observations, electrospray seems therefore advantageous to other thin film deposition techniques (Shui, 2004).

During an electrospray experiment, altering the applied electric field strength and/or the flow rate (the liquid kinetic energy) results in different electrospray modes. These modes differ in their droplet sizes and droplet formation mechanism. Among them, the cone-jet mode is the most studied one in thin layer production because of its ability to produce spherical particles, much smaller than the nozzle diameter, with a narrow size distribution (Agostinho, 2013; Jaworek et al., 2009). For the cone jet mode, scaling laws, for the electric current through the liquid and the droplet size, have been developed (Yuteri et al., 2010). The scaling laws depict that droplet sizes and final particle sizes can be easily controlled by adjusting different parameters, if we are indeed in the cone-jet domain with respect to flow rate and applied potential (Scheideler & Chen, 2014). With the advances in technology, this allows electrospray in the cone jet mode to find a wide application in different areas like microelectronics and nanotechnology (Jaworek &Sobczyk, 2008). Also depending on the physical and chemical properties of the liquid precursor such as density, surface tension, conductivity, concentration and viscosity, and experimental parameters like deposition temperature, deposition time, nature of the substrate, the surface morphology can be tailored (designed) to suit the preference (Neagu et al., 2006). These parameters are discussed in great detail in another section of this special issue (Rosell-Llompart et al., 2018; Ganan-Calvo et al., 2018). Obviously, the morphology of the deposited layer plays a crucial role in the final performance, e.g. for solar cells usually homogeneous flat layers are required while for ionic and electronic transfer from and out one layer to the other, rough layers are concerned in for instance battery electrodes.

Considering that the quality of a thin film depends on the particle sizes, their monodispersity and uniform distribution on the surface, electrospray is a powerful tool in material synthesis. The deposition parameters are extensively discussed in another part of this special issue (Jaworek et al., 2018; Bodnár et al., 2018)

Therefore, this review looks at different areas where the novel technique has been used to improve on the overall performance of materials for energy devices, which started with the paper of van Zomeren et al. (1994) for Li-ion batteries, and since then, more than 150 papers appeared on this subject. This amount is almost equal to the number of papers that arose on other energy device subjects discussed here, such as solar cells, photoelectrochemical cells, (O)LEDS including quantum dots, capacitors, and fuel cells. This last topic however, is described in another section of this special issue. (Castillo et al., 2018)

2 ESD for Energy Production (Solar Cells and Photo-Electrochemical Cells)

2.1 Solar cells

In solar cells, surfaces are often deciding the performance of the device in terms of light absorption and electronic behaviour. Hence, thin film fabrication methods are of utmost importance for achieving optimal operation of the solar cell. For the Si-based and GaAs solar

cells these depositions are typically based on vacuum methods and or oxygen- and moisture-free environments (sputtering, (PE)CVD, and (co-)evaporation). In contrast, potential future type solar cells like Copper Indium Sulfides/Selenides (CIS), perovskites (Fig. 1) and organic-type solar cells may use non-vacuum methods such as spin-coating, electro-deposition, screen-printing, doctor-blading, paste-coating, precursor-printing, and spray pyrolysis. (Shay et al., 1975; Mooney & Radding, 1982; Abernathy et al., 1984; Eberspacher et al., 2001; Panthani et al., 2008; Roncallo et al., 2008; Yoon et al., 2012)

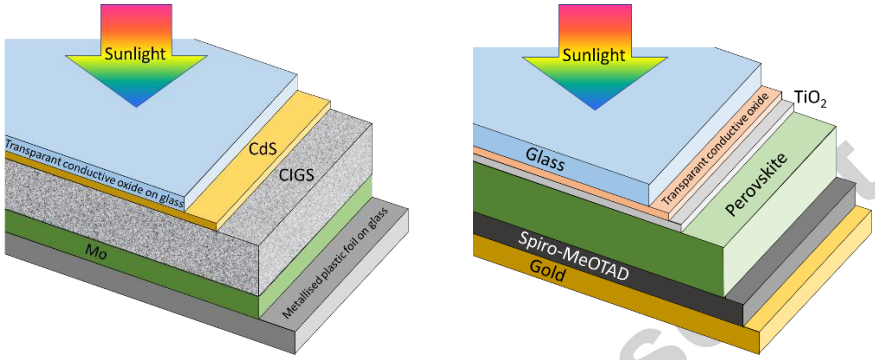

Fig. 1: CIS solar cell (left) and Perovskite solar cell (right).

Each of these methods has its pros and cons in terms of processing, chemistry, and final performance. For instance, spray pyrolysis was used by Mitzi et al. (2004, 2006, 2008, 2009) and Milliron et al. (2006) who deposited a Cu-In-Ga-Se (CIGS) layer, giving a solar cell power conversion efficiency of 10.3%. One of their precursors was hydrazine, and due to its reactivity and toxicity, it limits its widespread use. Ahn et al. (2010) coated a substrate with a $Cu(NO)_2$ and $InCl_3$ solution by using a doctor-blade method, but the efficiency was as low as 2%. In the following sections, an overview is given to address the issues in more detail by using ESD for fabrication of potential future solar cells based on CIS's, perovskites and organic materials. This paragraph also includes photo-electrochemical cells.

2.1.1 CIS-type solar cells

Table 1 (Yoon et al., 2012) summarises previous spraying studies for CIS based solar cells. These CIS-based solar cells are attractive because of:

- favourable optical and electrical properties: band gap tuneable from 1 to 2.4 eV by selection of the Ga to S ratio.
- high photon absorption coefficients,
- high power-conversion efficiencies compared to other systems.

Nevertheless, implementation of CIS-based solar cells is still hampered by high manufacturing costs as a result of the processing method via the earlier mentioned conventional vacuum deposition methods. Hence, non-vacuum-based deposition techniques would significantly reduce costs and may thus accelerate market penetration.

Table 1. Previous studies on $CuInSe_2$ solar cells produced by spraying solution-based precursors.(Yoon et al., 2012)

Solvent	Substrate	Deposition temperature	Conversion efficiency	Reference
ethanol/deionized water	pyrex	180-200 °C (<300 °C)	N.A.	Bougnot et al., 1986
ethanol	stainless steel	300-360 °C	N.A.	Shirakata et al., 1996

water, ethanol	pyrex, quatrz	350-550 °C	2%	Tomar & Garcia, 1982
1,2-propanediol	glass	300 °C	3.15%	Raja-Ram et al., 1986

Production of ESD CIS solar cells was shown with an initial low conversion efficiency (Yoon et al., 2012). Optimized precursor flow rates, which varied with the thermo-electrical properties of the dissolving solvents, were discussed. The effect of substrate temperature on the thin precursor films was also examined and are shown in Fig. 2. These precursor films then were selenized, performed in a vacuum evaporator equipped with a Knudsen-type effusion cell, at typically 530 °C for 30 min, under a Se flux regulated by the effusion cell temperature.

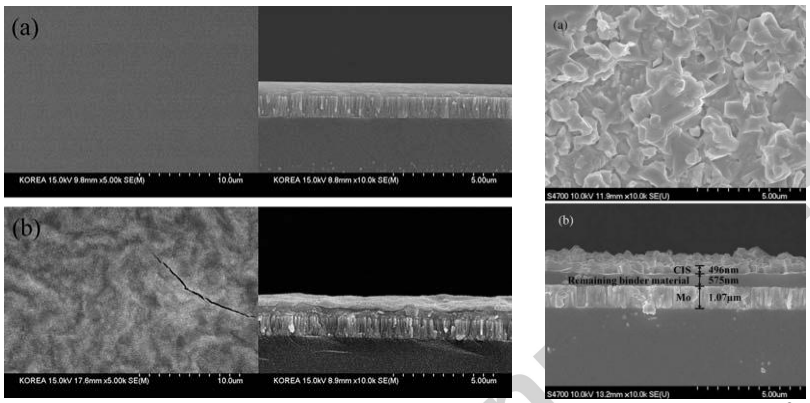

Fig. 2. Left panel: Morphologies of Cu-In films from propylene glycol solvent deposited at 100° C (a), and 200° C (b). Left and right images are top and side views, respectively. Right panel: (a) Top and (b) side views of a CIS thin film with selenium doping. Reprinted with permission from Yoon et al., 2012.

The deposition operating conditions that yielded the most uniform layer was used to produce cells for the necessary post-selenization process. The cells were then further covered with CdS and ZnO layers on top of the CuInSe layer. Light-illuminated current-density voltage (*J-V*) curves demonstrate a power conversion efficiency of η = 1.75% ± 0.09 with an open-circuit voltage of V_{OC} = 0.23 V, a short-circuit current density of J_{SC} = 21.72 mA/cm^2, and a fill factor *FF*=0.34 (Fig. 3) Room for improving the cell conversion efficiency by reducing or removing the carbon layer originating from our highly viscous solvents, was to be expected, as shown below.

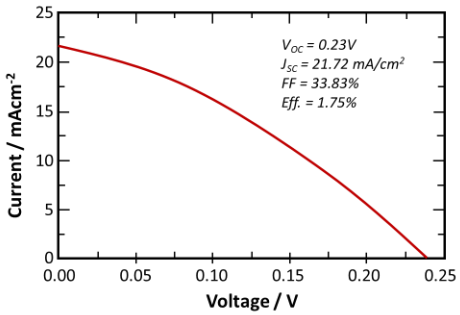

Fig. 3. I–V characteristics of the CIS solar cell on a molybdenum-coated substrate (Redrawn from Yoon et al., 2012).

The morphologies of the carbon- and oxygen-free Cu(InGa)$(SSe)_2$ (CIGSSe) absorber thin films prepared by ESD are shown in the left panel of Fig. 4. (Yoon et al., 2014) Similarly a

polycrystalline chalcopyrite CIGSSe absorber with a large-faceted flat-grained morphology was prepared after sulfurization and selenization and is presented in the right panel of Fig. 4.
7

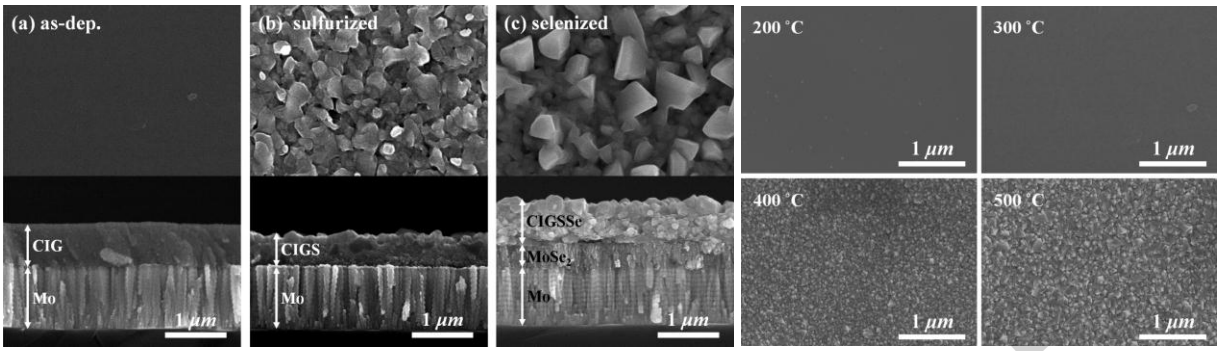

Fig. 4. Left panel: Top-view (top row) and cross-sectional (bottom row) SEM images of the (a) as-deposited CuInGa film, (b) sulfurized Cu(InGa)S2 film, and (c) selenized Cu(InGa)(SSe)2 film; Right panel: Top-view SEM images showing the effect of the airannealing temperature on the surface morphology and grain size of the as-deposited film (before sulfurization). Reprinted with permission from Yoon et al., 2014).

A solar cell with a 4.63% conversion efficiency was produced with V_{OC}= 410 mV, J_{SC} =21 mA/cm^2, and FF = 0.5337 for an active area of 0.46 cm^2 (Fig. 5).

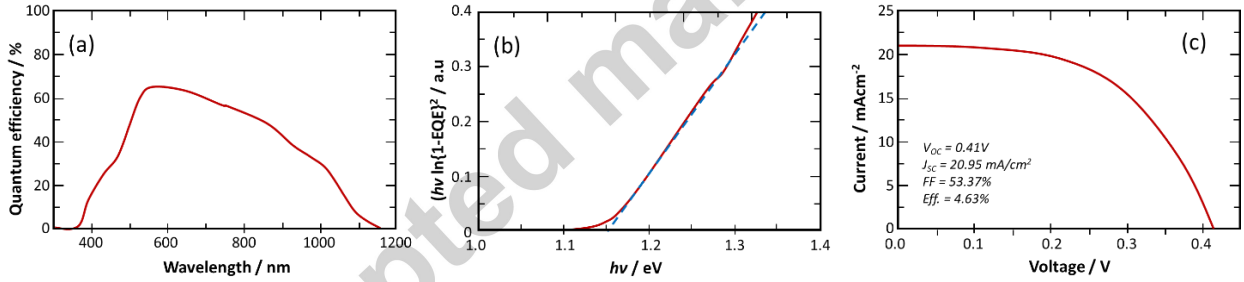

Fig. 5. (a) External quantum efficiency, (b) estimation of the band gap, and (c) I-V characteristics of the CIGSSe solar cell on a molybdenum-coated substrate. (Redrawn from Yoon et al., 2014)

Also, electrospun nanofibers were used to construct a 3D $CuInS_2$ solar cell with enhanced surface area on a ESD $CuInS_2$ layer (see Fig. 6). (Yoon et al., 2015) The electrospun CuInS film was annealed to crystalize the film, which was then sulfurized in a H_2S/N_2 environment to remove oxides. Both XRD and Raman characterization confirmed the formation of $CuInS_2$. SEM images (Fig. 6) revealed a 3D web-like, fibrous structure of the film. AFM data showed that the surface area had nearly doubled after incorporating the 3D nanostructure. The solar cell has a standard Mo/CIS/CdS/i-ZnO/n-ZnO/Al structure.

Finally, the fabricated CIS nanofiber cell had a V_{OC}=0.21V, J_{SC}=9.07mA/cm^2, FF=35.64% (Fig 7), and a conversion efficiency of 0.66% with an active area of 0.44cm^2. The low efficiency was attributed to a limitation in the TCO sputtering process, which did not yield a complete penetration of the transparent conductive oxide (TCO) materials into the open pores between CIS/CdS fibers, which may eventually be improved by using metal nanowires together with indium tin oxide (ITO) nanoparticles.

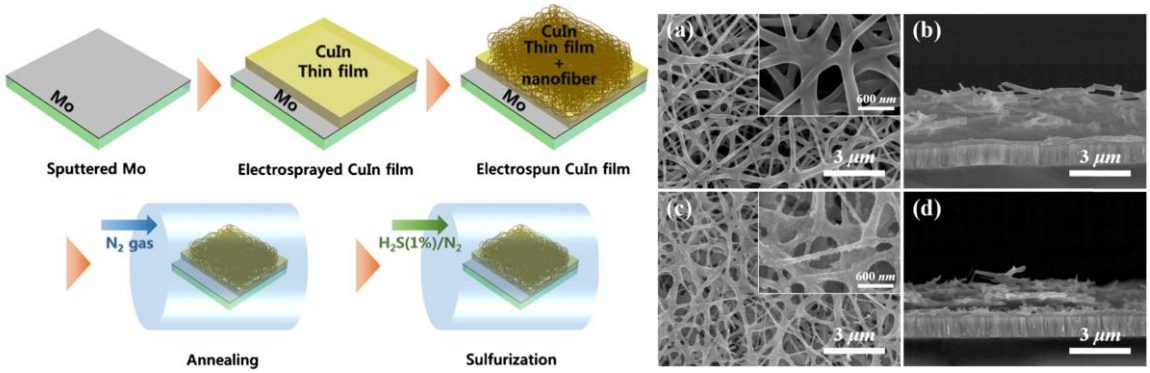

Fig. 6. Fabrication of 3D nanostructured CIS (left), and SEM image of annealed (a and b) and sulfurized (c and d) 3D nanostructured CIS absorber layer. Reprinted with permission from Yoon et al., 2015.

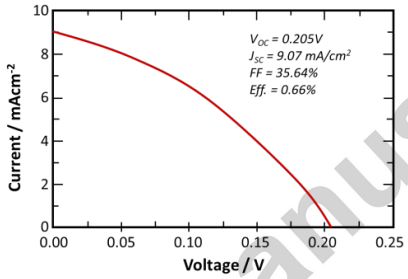

Fig. 7. I–V characteristics of the CIS solar cell on a Mo-coated substrate. (Redrawn from Yoon et al., 2015).

A low cost, scalable electrostatic spray assisted vapour deposition (ESAVD) method using DMSO as solvents was employed to deposit Copper-Zinc-Tin-Sulfide (CZTS) absorbers (Altamura et al., 2015). In order to further improve the efficiency, an ultrathin ZnO intermediate layer was deposited between CZTSSe and Mo to minimize absorber decomposition at the back contact surface. The thin ZnO layer no longer existed after treatment with selenium (SEM images in Fig. 8) because Zn was incorporated into the CZTSSe absorber and O was replaced by Se (Sample I).

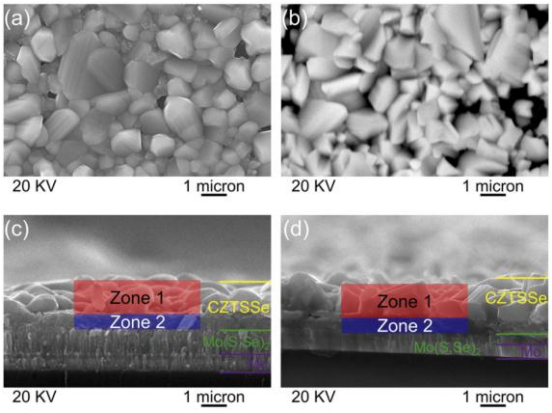

Fig. 8. Top-view and cross-section SEM images of CZTSSe after selenium treatment for Sample I (a, c) and Sample II (b, d). Reprinted with permission from Altamura et al., 2015.

The reaction between ZnO and Se vapour reduced the thickness of high resistance Mo(S,Se) layer formed during selenization. For another sample (Sample II) with a thin ZnO intermediate layer, the Zn/Sn ratio after selenization was lower than the reference sample. It was concluded that preventing decomposition of CZTSe in the vicinity of the Mo back contact allows a reduction of the loss of Sn during the annealing, which suggests the existence of a relationship between the loss of Sn and the formation of secondary phases at the back region of the absorbers. Comparison between Raman spectrum of Sample I and Sample II proved that a thin ZnO layer successfully reduced the decomposition of CZTSSe at the back contact surface. The improvement of the CZTSSe|Mo interface due to the intermediate layer was also reflected in the quality of the derived photovoltaic devices leading to an improved efficiency for ESAVD-deposited kesterite of 4.03% with ESD.

2.1.2 Perovskite-based solar cells (PSCs)

Within the last years, perovskites have made enormous progress as solar cell materials, with a power conversion efficiency reaching up to 17%, (Jeon et al., 2014; Lee et al., 2014; Nie et al., 2015; Jeon et al., 2015), or higher when based on a planar architecture containing mixed halide perovskite ($CH_3NH_3PbI_{3-x}Cl_x$) materials (Zhou et al., 2015), and beyond that (http://www.nrel.gov/ncpv/images/efficiency_chart.jpg). Hence, PSCs are becoming highly interesting next generation solar cell devices for converting solar energy. Unfortunately, PSCs show severe problems with respect to incorporated defects leading to a hysteresis in the I–V characteristics (Nie et al., 2015). Thus, improving the perovskite film surface coverage is an important field, where the process plays a crucial role. Several techniques were reported to obtain large crystals with uniform perovskite films, via solution methods, (Uurschka et al., 2013; Docampo et al., 2014; Jeon et al., 2014) thermal evaporation, (Liu et al., 2013) and spray coating (Barrows et al., 2014; Ramesh et al., 2015), including either a one-step solution or a two-step sequential deposition technique to obtain uniform, and dense perovskite films (Nie et al., 2015; Jeon et al., 2014). A modified two-step sequential deposition method (solution–vapour) was used by initially spin coating followed by vapour deposition (Hu et al., 2014; Xiao et al., 2014). Unfortunately, these methods reveal serious disadvantages:

- waste of precursor materials
- formation of island like perovskite structures creating reduced surface coverage with pinholes
- incomplete conversion of the precursor leads to formation of poor quality perovskite films.

In order to make perovskites more attractive for market implementation, control of the deposition is important. Usually, spray methods lead to small grain size and thus pin hole formation, but also to incorporation of impurities (Krishna et al., 2003). Hence, in order to achieve enhanced electronic properties, the morphology and crystallinity of the perovskite films need to be improved. It is however stressed that the method used was performed with voltages that does not allow actual electrospraying, but uses merely a high voltage as assistance to the standard spraying (Fig. 9) (Chandrasekhar et al., 2016). Nevertheless, deposition may be expected with full electrospraying as well.

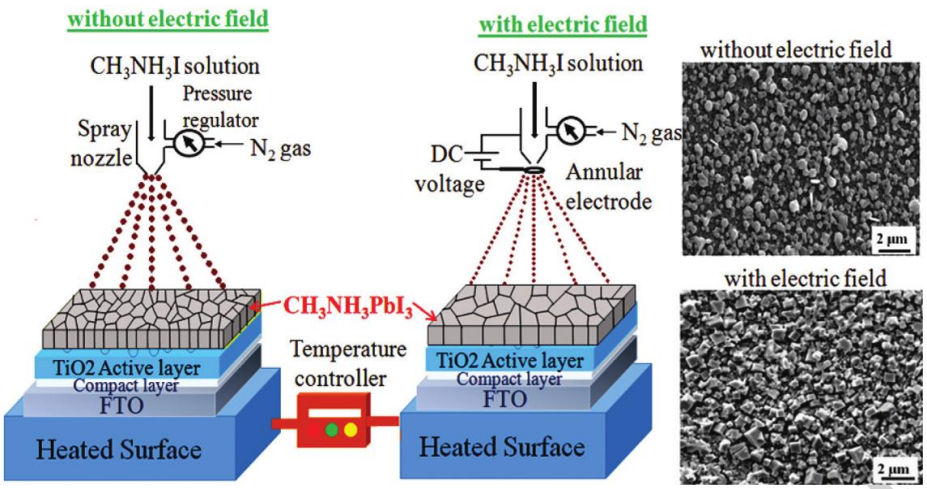

Fig. 9. Scheme of the spray deposition process of perovskite films with (2kV) and without electric field, together with the corresponding film surface morphologies. Reprinted with permission from Chandrasekhar et al., 2016.

2.1.3 Organic solar cells

In Organic Photovoltaic (OPV) devices typically photogenerated excitons are dissociated by the photovoltaic energy gap, and then the charges are separated by the built-in potential created the electrodes. In order to do so, the electrode layers need to be well-adjusted so as to make sharp interfaces at the p-n junction. The processing allows similar critical issues as required for the deposition of (O)LEDS, and thus will be discussed there. Most recently, ESD has been used to fabricate OPV layers of P_3HT:PCBM active layers with bulk heterojunction (Kim et al., 2010; Fukuda et al., 2011; Fukuda et al., 2012; Park et al., 2011; Kim et al., 2012) and multi-layer structures (Ali et al., 2012), but also as to deposit poly(3,4-ethylenedioxythiophene): polystyrene sulfonate (PEDOT:PSS) as hole transport layer (Kim et al., 2012) or as an electrode (Kim et al., 2012). An active layer of P3HT:PC61BM led to a PCE of ~3.00% using acetic acid as additive in ESD, which is comparable to that of the OPV device fabricated by spin coating (Zhao et al., 2014). A molecular ordered uniform P3HT:PCBM thin film with the high crystallinity deposited by ESD showed a PCE of 2.0% (Fukuda et al., 2016). Ordered PTB_7-Th:PC71 BM polymers with specific sizes were fabricated via ESD to form thin films. By optimizing solvent evaporation and thickness of the layers, a power conversion efficiency (PCE) of 8.6% was obtained. Very recently ESD was applied to fabricate a multilayered (three-component) device structure (Fukuda et al., 2017).

2.2 Photoelectrochemical Cells

Photoelectrochemical cells (PECs) are solar cells that provide electricity to typically produce hydrogen via electrolysis of water, i.e. water splitting (Fig. 10).

The active electrode is often a modified TiO_2 layer. Dye-sensitized solar cells prepared by ESD immersed in aqueous solution (Fujimoto et al., 2006), with a I_3^- electrolyte, showed higher J_{sc} than those prepared by conventional coating methods, which was assigned to the presence of a better ionic path in the TiO_2, due to the specifically formed morphology. The results are shown in Fig. 11.

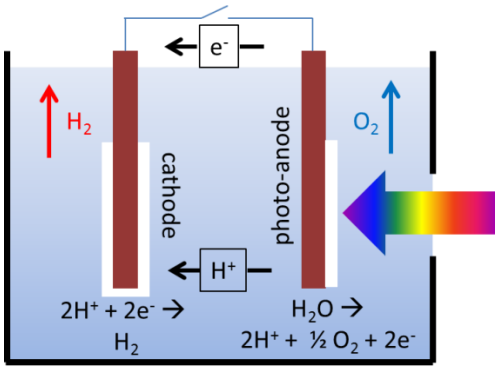

Fig. 10. Photo-electrochemical cell.

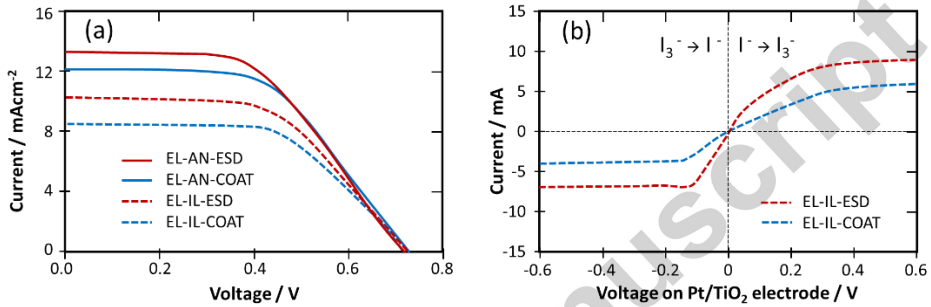

Fig. 11. (a) I-V curves for dye-sensitized solar cells fabricated with conventional coating (COAT) and ESD. EL-AN and EL-IL stands for acetonitrile (AN) and ionic liquid (IL) electrolyte (EL), respectively. All film thicknesses were 9 µm. (b) Limiting current measurement for cells with a TiO_2 layer prepared by conventional coating and ESD. Redrawn from Fujimoto et al., 2006.

ESD was also used to deposit CdSe QDs onto nanostructured TiO_2 films to form a photovoltaic cell electrode (Li et al., 2015). Compared to conventional processes like dip coating with linker-containing molecules or chemical bath deposition, ESD has shown uniform deposition of QDs as mentioned earlier, and here it is used to cover a nanostructured TiO_2 surface without linker-molecules. ESD allows preserving the physical and the optical properties of the QDs. To optimise the final energy conversion efficiency for the photolysis of water, various different concentrations and deposition times were employed. The as-deposited films were annealed later on, to ensure binding between the QDs and the TiO_2 surface. Despite that a small number of deposited QDs limit the number of absorbed photons, multiple layers of QDs cause more defects and trap sites enhancing electron-hole recombination ascribed to inhibition of the transportation of photo-generated electrons into TiO_2.

Beside the standard TiO_2 material, Nanostructured spinel zinc ferrite ($ZnFe_2O_4$) thin films were prepared on transparent conductive substrates via ESD at 400 °C, followed by annealing (Wang et al., 2017). The $ZnFe_2O_4$-film thickness played an important role in the PEC performance, where porous thin films with an enlarged interfacial area between $ZnFe_2O_4$ and the electrolyte were obtained, which led to an increased discharge potential, due to an increased number of active sites giving an enhanced photocurrent of 53 µA/cm^2 at 1.23 V versus RHE.

3 ESD for Energy Storage (*Batteries and Capacitors*)

3.1 Lithium ion batteries (LIBs)

Today, Li-ion batteries are the major rechargeable electricity carriers for consumer electronics and also electric vehicles, and might be in the near and/or long future. In Fig. 12 a scheme of the working principles of a Li-ion battery is presented.

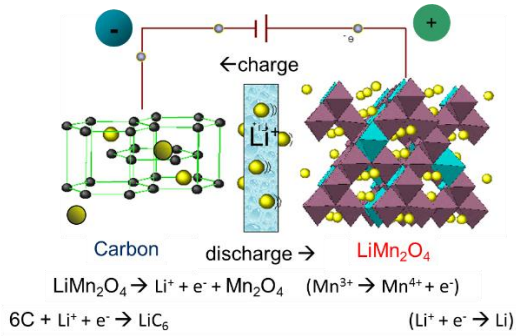

Fig. 12. Li-ion battery principles with a $LiMn_2O_4$ cathode and carbon anode as an example.

Both electrode materials, positive and negative, can be and were synthesized using ESD. For the positive electrode layered structures ($LiMO_2$, with M any combination of transition metal ions), spinels (LiM_2O_4, with M any combination of transition metal ions), and olivines ($LiMPO_4$, with M typically a combination of iron and cobalt ions) were identified. For the negative electrode all sorts of transition metal oxides are being tested as well as many metals and alloys. Both have been made via ESD, either via composites with spraying the actual powder, or via a chemical deposition reaction during spraying. The performances of the materials are typically measured on flat coatings, so as to reduce the influence of the interface between the electrode and electrolyte, as well as to accurately measure the surface area of the interface. Here an overview is given of several materials with respect to surface morphology and composition for positive electrodes. With respect to negative electrode materials synthesized by the ESD, an thorough review was written by Li & Wang (2013). The attention there was focused on three different anode categories: (1) insertion anodes, such as graphite, $Li_4Ti_5O_{12}$ and TiO_2, etc.; (2) alloying–de-alloying anodes, such as Sn and SnO_2, etc.; and (3) conversion reaction anodes, such as NiO, Fe_2O_3, Co_3O_4, CoO, and Cu_2O. Hence, this part will not be further discussed here.

ESD was employed to fabricate various morphologies of cathode materials for Li-ion batteries as reported by Chen et al. (1996). Since then, many other cathode materials having several different morphologies (Sun et al., 2013) have been formed and described in the literature. It is stressed that in order to characterize various materials properties, flat surfaces are often used. These properties comprise structural information (XRD, IR-RAMAN, etc) and electrochemical information (e.g. diffusion coefficients, ionic and electronic conductivities) (Nishizawa et al., 1998; Dokko et al., 2004; Mohamedi et al., 2002; Chung et al., 2004; Shu et al., 2003; Chung et al., 2005).

Since charge transfer of either electrons or ions is an important issues for electrodes in devices, the morphology of it, is of utmost importance, because it will reflect the exchange area of these charge carriers. Here a short overview of the electrode performance will be given on the basis

of flat, rough (porous), and reticular structures, also with respect to their composition. Since there are so many different process parameters to vary in order to obtain a certain layer, it is too difficult to make a well-justified comparison, also in the light of the length of the paper. Nevertheless, several results are given so as to show the actual importance of the various morphologies on cathode performance.

For the layered structures $LiMO_2$, $LiCoO_2$ has been taken as a positive electrode material example (Yoon et al., 2001; Koike & Tatsumi, 2007). It is clear from Fig. 13 and Fig. 14 that the capacity of the most porous structure is significantly higher than the non-porous structure. The power performance of those layers are also found to be higher than the non-reticular ones. This is a phenomenon that has been observed for most of the reticular structures compared to the flat or other rough and porous structures.

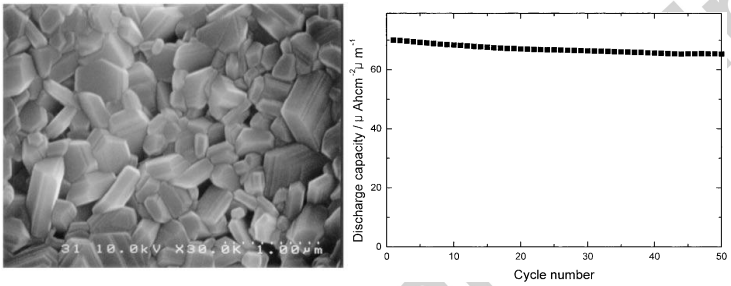

Fig. 13. (a) SEM of $LiCoO_2$ film annealed at 600 C and (b) Cycle performance. Reprinted with permission from Yoon et al., 2001.

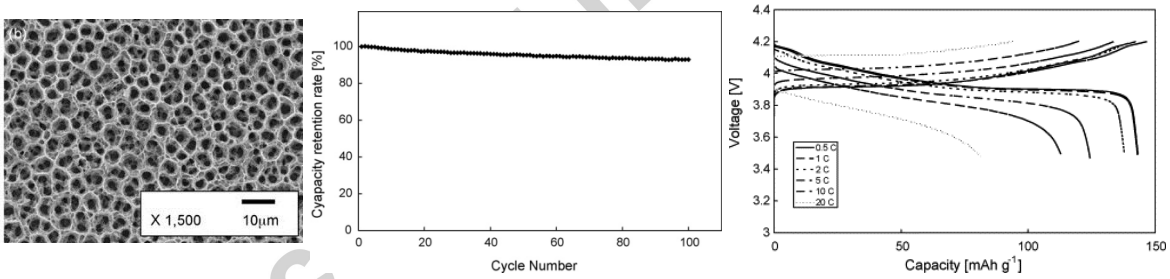

(a) *(b)* *(c)*

Fig. 14. (a) SEM images of surface morphologies of $LiCoO_2$ films prepared by ESD after heat treated at 650 ^oC for 2 hours, (b) cycle performance and (c) rate performance. Reprinted with permission from Koike & Tatsumi, 2007.

In order to further improve the performance of the films, the materials were coated (Shu et al., 2003) or modified with an indifferent additive such as nano-particles of silica (Fig.15) (Yu et al., 2006). With the latter, an improved performance is clearly observed.

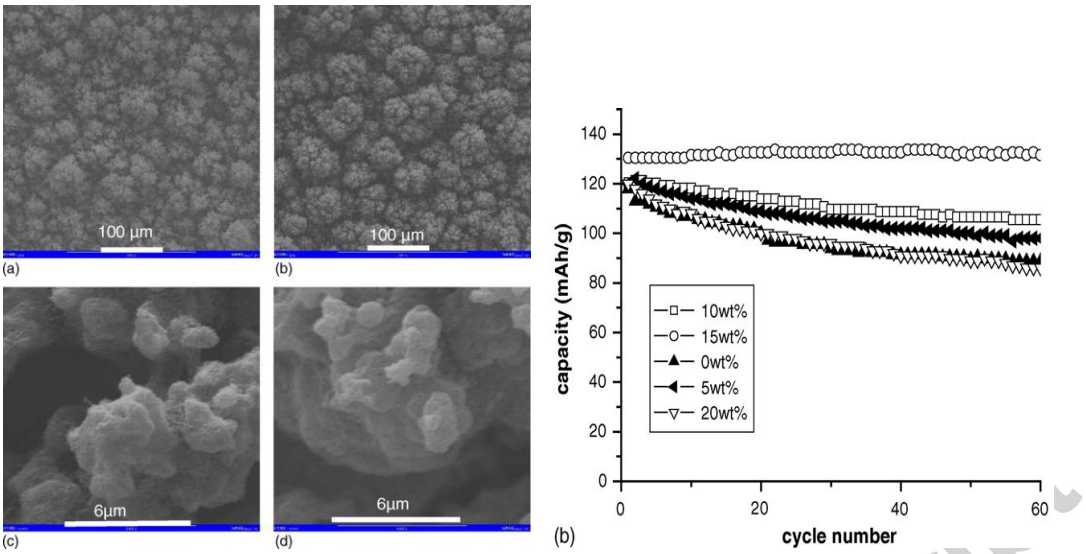

Fig.15. Left panel: scanning electron microscopy pictures of a $LiCoO_2$ thin film (a and c) and a $LiCoO_2$–15 wt% SiO_2 thin film (b and d). (69). Right panel: capacity and cycle performance as a function of silica content. Reprinted with permission from Yu et al., 2006.

Obviously, the layered structures can be further improved by stabilising the structures by replacing certain amounts of cobalt by other transition metal ions or aluminium. For example, $Li(Ni,Co,Ti)O_2$ compounds was prepared by ESD with a combinatorial method (Fig. 16). (Fujimoto et al., 2007; Fujimoto et al., 2011)

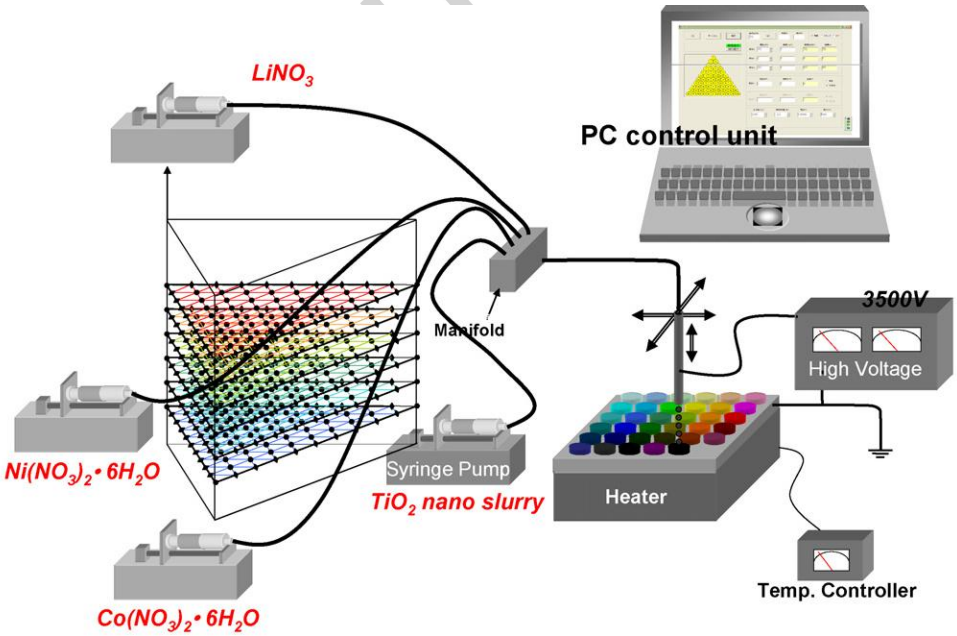

Fig. 16. Scheme of the so-called M-ist Combi system based on an electrostatic atomization method. Reprinted with permission from Fujimoto et al., 2007.

The charge–discharge characteristics of the Li(Ni,Co,Ti)O_2 powder were recorded in a voltage range from 4.2 to 2.8 V at 1C and those were found to retain their capacity better than pure $LiCoO_2$ at the same C-rate (Fig. 17).(Fujimoto et al., 2011)

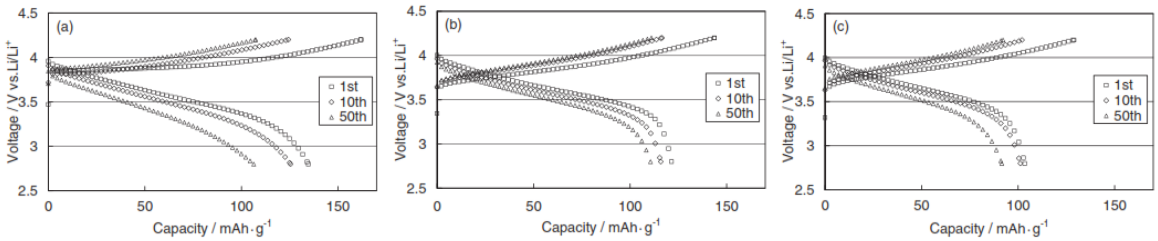

Fig. 17. Charge–discharge curves of $LiNi_{0.4}Co_{0.6-x}Ti_xO_2$ electrodes: (a) x = 0, (b) x = 0.1 and (c) x = 0.2. Reprinted with permission from Fujimoto et al., 2011.

Despite the great performance of the reticular structures for a 3D solid state battery a dense flat coating on a high aspect ratio surface is important for fast electronic charge transfer, which may be problematic for the reticular structures as the contact area with the current collector is minimal. The advantage of ESD in that respect is that the it is possible to coat surfaces with aspect ratios of 10, as shown in Fig. 18 with $LiNi_{0.5}Mn_{1.5}O_4$ electrode material. (Lafont et al., 2012). It is stressed that in Fig. 18d , the cross-section was taken along the red line of Fig. 18c.

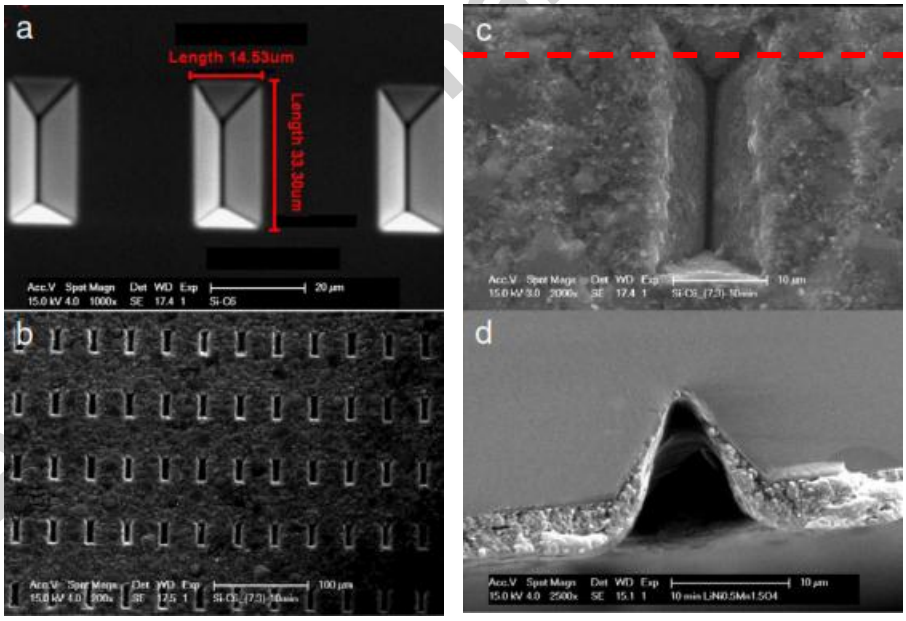

Fig. 18. SEM images of Si wafer showing 3D architecture (a) before and (b, c) after film deposition. (d) Cross section along the red dotted line of c) showing the film thickness. Reprinted with permission from Lafont et al., 2012.

The $LiFePO_4$ olivine cathode materials are of interest today, but not much has been reported on ESD for these materials, most likely because the production of the material itself usually occurs under certain strict atmospheres, which makes it difficult to deposit these layers in one step. Nevertheless, its counterpart, $LiCoPO_4$ (Yu et al., 2006) was fabricated where the impurities

Li_3PO_4 and Li_3PO_4 work as protective coating and electronic enhancer, respectively (Fig. 19). (Shui et al., 2006)

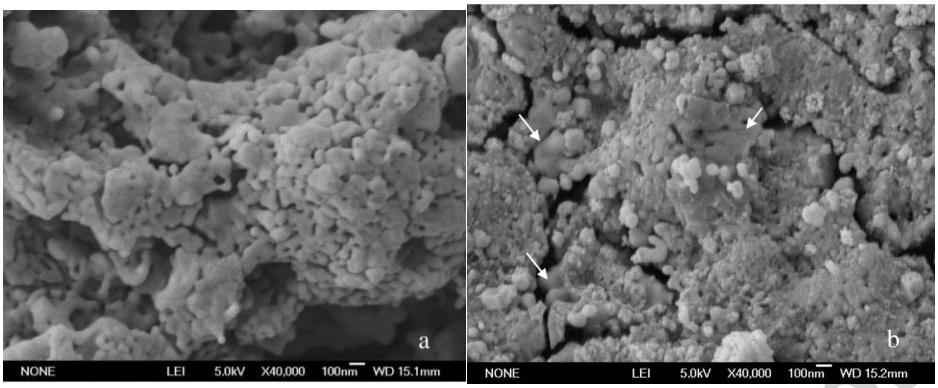

Fig. 19. SEM images of ESD syntheszsed $Li_{1.0}CoPO_4$ '' (a) and $Li_{1.8}CoPO_4$ (b) films. The arrows in (b) indicate the uncovered areas. Reprinted with permission from Shui et al., 2006.

Another advantage of ESD is to form composite layers. Several papers reported on improving the electrode performance by depositing composite electrodes either anodes or cathodes (Garcia-Tamayo, et al., 2011; Cho et al., 2016; Wu et al., 2015; Danabalan et al., 2013Damien et al., 2016). These improvements are then explained by an increase in the electronic and ionic migration processes induced by the interfaces created between the electrode material and the additive.

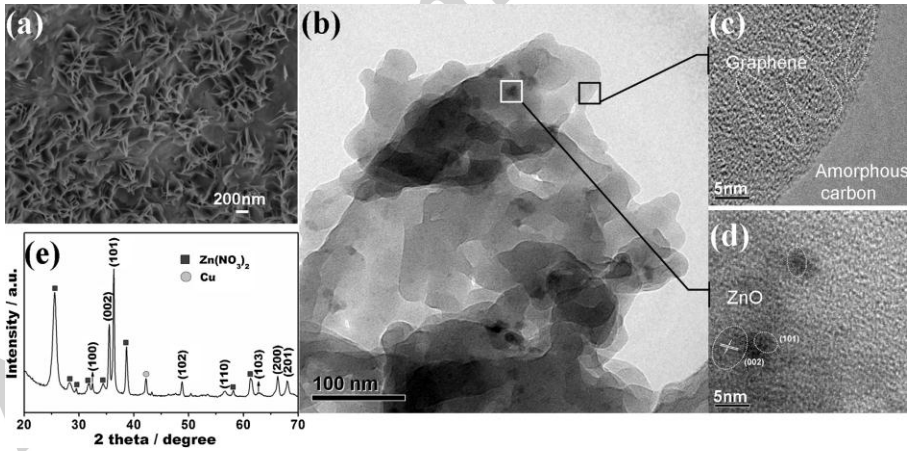

Fig. 20. SEM (a) and TEM, (b) images of nanostructure ZnO/rGO composite films; HRTEM of rGO, (c) from light area and ZnO, (d) from dark area; and XRD pattern, (e) of ZnO/rGO deposited on copper substrates by ESD. Reprinted with permission from Wu et al., 2015.

3.2 Beyond Li-ion batteries

3.2.1 Na-ion batteries

The high energy density of batteries and the high power density of supercapacitors are combined in a self-supported interpenetrating 3D tricontinuous $Na_3V_2(PO_4)_3$-rGO-CNT cathode made via ESD, where the cathode is directly deposited on the current collectors without any conductive additives or binders (Zhu et al., 2016). The $Na_3V_2(PO_4)_3$-rGO-CNT material used as an

anode as well as a cathode shows outstanding rate capability and long cycling stability (Fig. 21). At a current density of 100C, the sodium cathode can still deliver a specific capacity of 82 mAh/g (~70% theoretical capacity), which is almost as high as observed for supercapacitors but with a much higher energy density. It also shows an outstanding cycling stability, as at a current density of 10C, the capacity still maintains 96% of its initial capacity, even after 2000 cycles.

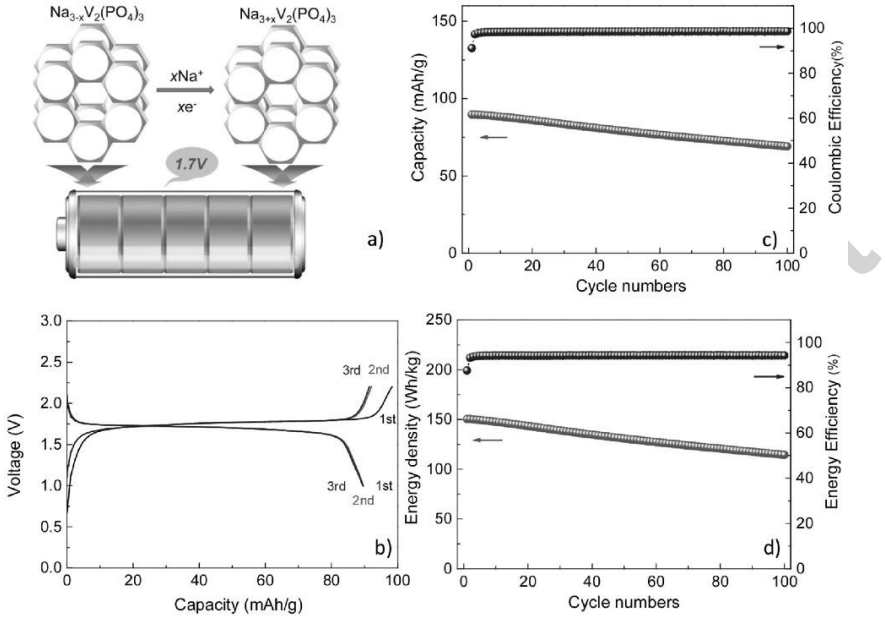

Fig. 21, a) Scheme of a symmetric full sodium battery using interpenetrating 3D tricontinuous NVP:rGO-CNT as both positive and negative electrodes. b) Galvanostatic charging–discharging profiles for the first three cycles at 10C. c) Cycling performance and Coulombic efficiency for 100 cycles at 10C. d) Discharge energy density and energy efficiency at 10C versus cycle numbers. Reprinted with permission from Zhu et al., 2016.

A freestanding alluaudite $Na_{2+2x}Fe_{2-x}(SO_4)_3$@porous carbon-nanofiber (PCNF) hybrid film is fabricated by combining electrospinning and ESD (Yu et al., 2016). The obtained highly porous graphitic-like carbon-nanofibers intimitaly enveloppes the sulfate nanoparticles, resulting in a hybrid sulfate@PCNF network. This conductive network shows a very flexible and stable architecture, where the freestanding film demonstrates fast electron/ion transport and superior cycling stability, capable of high rate ultralong-term cycling. It retains more than 95% of its initial capacity even after 500 cycles at rates up to 40C (Fig. 22).

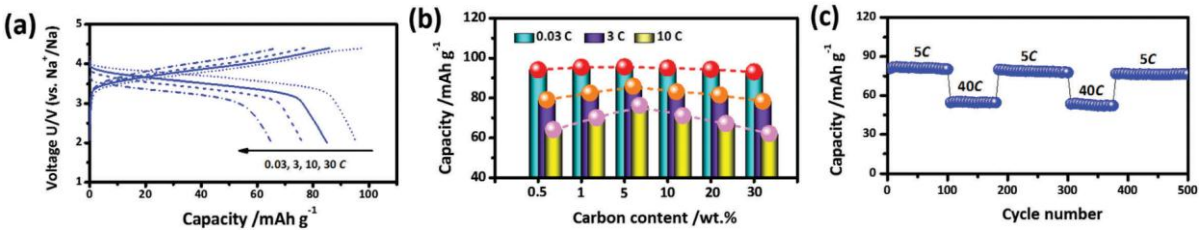

Fig. 22 (a) Galvanostatic charge/discharge curves of the hybrid nanofibers at various rates: 0.03C, 3C, 10C and 30C. (b) Comparison of discharge capacities at different current densities for the hybrid nanofibers with various carbon contents. (c) High-rate and long-term cycling properties of the hybrid nanofiber. Reprinted with permission from Yu et al., 2016.

3.2.2 Li-sulfur batteries

Ultrathin multifunctional coatings (~100 nm) on cathodes for a Li-S batteries which will effectively block polysulfide shuttling has been fabricated by ESD (Niu et al., 2016). This layer warrents fast ion diffusion without adding too much to the volume or weight, and prevents sufficient blocking of polysulfides to arrive at the counter electrode so as to avoids shorts (Fig. 23).

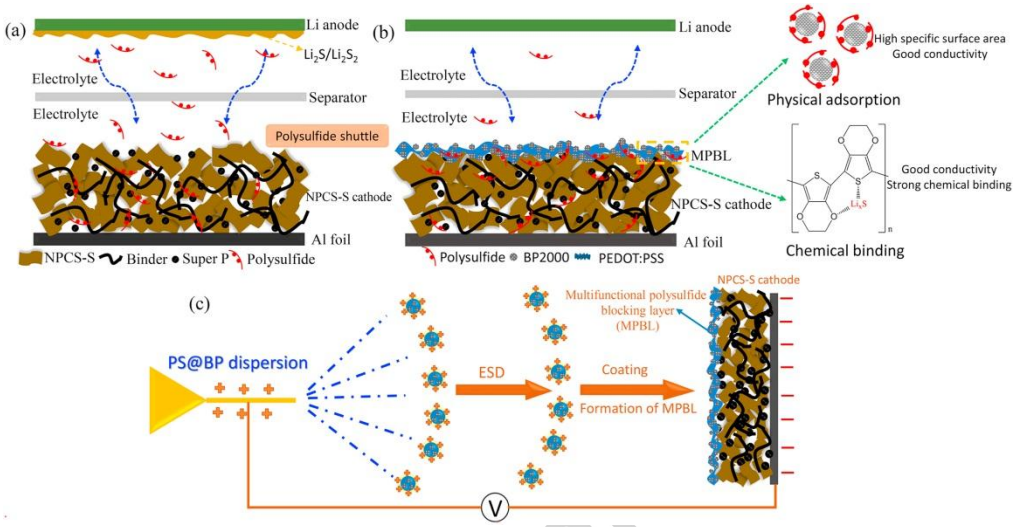

Fig. 23. Scheme of the electrode configurations for (a) a conventional uncoated cathode and (b) a MPBL-coated cathode for Li-S battery. (c) Scheme of the procedure for fabricating a MPBL-coated electrode. Reprinted with permission from Niu et al., 2016.

Black Pearl 2000 was uniformly dispersed in mixtures of water and ethanol (1:1 (V/V)) via sonication, to which PEDOT:PSS was added (Niu et al., 2016). This suspension was thus sprayed at 10mL/h with a nozzle (20 gauge size) at 21 kV with a substrate to nozzle distance of 5 cm for 5 mins to form a uniform MPBL coating (Fig. 24). The multifunctional polysulfide blocking layer (MPBL) exhibits a good cycling performance with only 0.042% capacity decay per cycle at 1C for 1000 cycles and an excellent rate performance with a high capacity of 615 mAh/g at 3C.

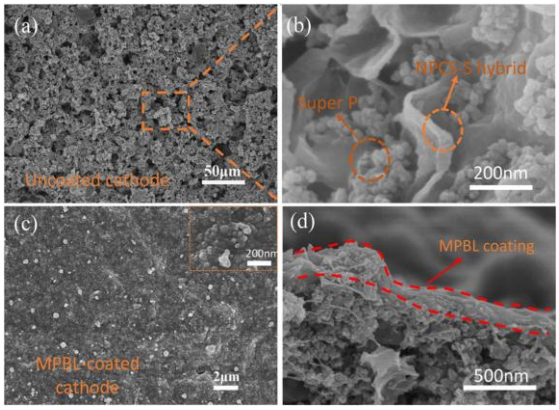

Fig. 24. (a, b) SEM images of uncoated hybrid nitrogen-doped porous carbon sheet (NPCS-S) cathode. (c, d) Surface and cross-section SEM images of the MPBL-coated NPCS-S cathode. Reprinted with permission from Niu et al., 2016.

3.3 Capacitors

Electrochemical capacitors (ECs), also known as supercapacitors or ultracapacitors, gained enormous interest as potential power source for the future smart energy era, due to their high power density, long life cycle, and high rate capacity (Largeot et al., 2008; Pognon et al., 2011). In order to achieve that a higher energy density without influencing other electrochemical properties is required. Among the electrode materials, metal oxides provide higher energy densities than conventional carbon materials and showed improved electrochemical stability over polymer materials. This carbon based material for micro-capacitors, however, showed interesting performance made via ESD. On the other hand, the low electrical conductivity of oxides has significantly influenced their performance (Wang et al., 2010; Lee et al., 2005; Wu et al., 2011). A combination of both, such as graphene metal oxide composites has shown great potential for application in ECs due to their improved electrical conductivity, large specific surface area and excellent electrochemical stability (Zangmeister, 2010; Qu et al., 2012; Zhang et al., 2010; Mao et al., 2012). The challenge is thus to form these graphene-based materials as restacking during the preparation process is an issue: the strong π-π interactions in graphene oxide (GO) usually results in irreversible precipitated agglomerates forming its reduced form (rGO). The agglomeration usually decreases the active surface area and thus prevents the access of electrolyte ions into graphene sheets, deteriorating the final performance (Zhang et al., 2010; Mao et al., 2012). This problem might be circumvented by applying ESD. In the following part, carbon-based electrode materials, manganese oxide, ruthenium oxide, titanium-vanadium oxides, nickel oxide, and vanadium oxide composite electrodes made via ESD are summarised.

3.3.1 Carbon electrode materials for capacitors

Binder-free reduced graphene oxide (rGO)/carbon nanotube (CNT) hybrid thin film electrode were made using one-step ESD (Youn et al., 2014). Here the carbon nanotube was used as a nano-spacer to improve the electrochemical properties of the rGO/CNT hybrid thin film electrode, by sandwiching the CNT between the 2D rGO layers, so as to prevent restacking of the rGO sheets (Beidaghi & Wang, 2012). This was achieved by using a uniformly dispersed colloidal suspension of GO and CNTs in a mixture of water and ethanol by ultra-sonication. This dispersion then was used for the formation of the electrode by ESD with a suspension flow rate of 8-15mL/h on a Pt-coated Si-wafers at 10-15kV and 300°C. Thus, sandwiching the CNT (Fig. 25) in the hybrid electrode increases the electrochemically effective surface area and also prevents agglomeration (restacking) of the rGO sheets. Cyclic voltammetry, galvanostatic charge/discharge test and electrochemical impedance spectroscopy, showed that the rGO/CNT hybrid electrode had better electrochemical performance than a plain rGO electrode in terms of specific capacitances and rate capabilities. The thin film electrode has a higher reversible specific capacitance of 187F/g at 0.5 A/g and performed better having a rate capability and even showing 73% of the specific capacitance at 16A/g (vs. 0.5 A/g) (see Fig. 26).

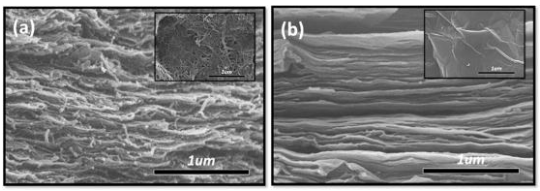

Fig. 25. SEM images of the rGO/CTN hybrid thin film; (a) cross-section view (Inset: basal plane view) and those of the rGO thin film electrode; (b) cross-section view (Inset: basal plane view). Reprinted with permission from Youn et al., 2014.

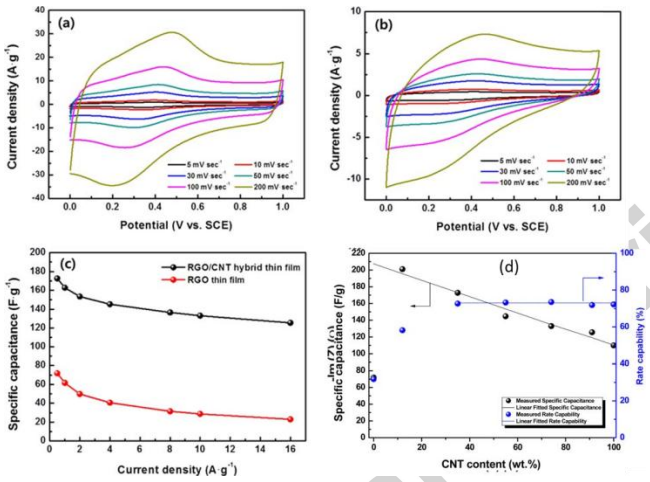

Fig. 26. Cyclic voltammograms of (a) the rGO thin film electrode and (b) the rGO/CNT hybrid electrode at various scan rates (5-200 mV·sec). (c)The rate capabilities of the rGO thin film and rGO/CNT hybrid thin film electrode. (d) Specific capacitance and high rate capability of the rGO/CNT hybrid electrodes as a function of CNT content, pure rGO and pure CNT electrodes. Reprinted with permission from Youn et al., 2014.

In another study, thin-film electrodes of graphene nano-platelets (GNPs) were fabricated with ESD. This combination of binder-free ESD using an open pore structure of graphene films results in an excellent power performance of the electrodes, as shown by cyclic voltammetry which showed almost rectangular curves even at a very high scan rate (Fig. 27). (Beidaghi et al., 2012) A specific power and energy of about 75.46 kW/kg and 2.93Wh/kg, respectively, at a 5V/s scan rate was obtained for 1 µm thick electrodes, and about 53 % of the initial specific capacitance of electrodes at low scan rates was retained at a scan rate of 20 V/s. The thickness of the thin-film electrodes had some influence on the rate capability, but even an electrode with an thickness of 6 µm retained about 30 % if its initial capacitance at a very scan rate of 20 V/s. Hence, the GNP electrodes made with ESD proved to be promising as thin-films for energy storage.

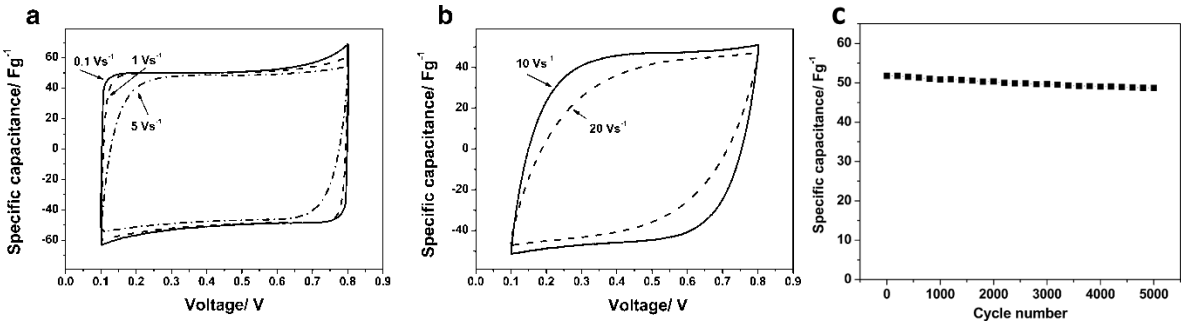

Fig. 27. Cyclic voltammograms recorded in 1 M Na_2SO_4 (vs. Ag/AgCl) of GNP electrodes at scan rates ranging from 0.1 to 20 V/s of a 1-µm-thick electrode (a, b). Cyclic stability tested at a 0.1-V/s CV scan rate (c). Reprinted with permission from Beidaghi et al., 2012.

3.3.2 Carbon nanotube (CNT) film electrodes

CNT film electrodes were fabricated by ESD from a CNT suspension, where acid treated CNTs were dispersed in an aqueous solvent through sonication. This suspension then was sprayed onto a metallic substrate (Kim et al., 2006). The thin film electrodes showed well-entangled and interconnected porous structures which adhere well to the metallic substrate (Fig. 28). A specific capacitance of 108 F/g was obtained for the electrodes in 1 M H_2SO_4 at high rate capability (Fig. 28).

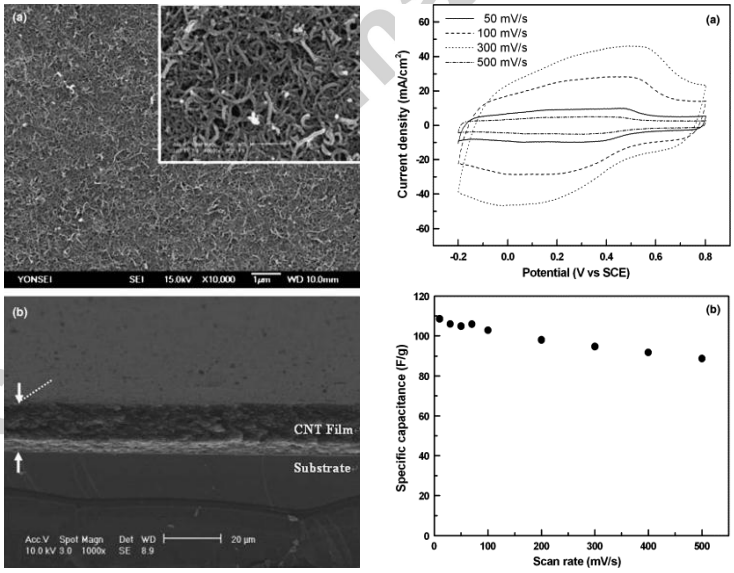

Fig. 28. Left panel: SEM images of (a) plane and (b) cross section views of CNT film electrode. Right panel: (a) Cyclic voltammograms and (b) specific capacitance of a CNT film electrode as a function of the potential scan rate. Reprinted with permission from Kim et al., 2002.

3.3.3 Mn_xO_y electrode materials

The focus here is on nanostructured manganese oxide layers without carbon additives deposited on stainless steel substrates. The electrochemistry of the layers is mainly affected by the MnO_2 morphology, resulting from the spraying conditions. The preferred stoichiometry of the manganese oxide is MnO_2, with a valence of 4+. A thermal treatment alone on the layers

was not sufficient, but further oxidizing to MnO_2 by electrochemical means, revealed a significant improvement of the capacitance properties (Fig 29a). This was explained by a change in morphology upon electrochemically annealing, leading to fine MnO_2 nanorods. The actual redox reactions are then:

$$MnO_2 + xNa^+ + yH^+ + (x+y)e^- \leftrightarrow MnOONa_xH_y$$

The specific capacitance measured with cyclic voltammetry decreased of the non-electrochemically treated samples runs from 330 down to 150 F/g with increasing loading of the active mass, i.e. 18 to 116 µg/cm^2, respectively (Marsalek et al., 2015). The electrochemically oxidized layers exhibited specific capacitances over 150 F/g (Fig. 29), which are comparable to the results published by other research groups, but here made with less expensive materials.

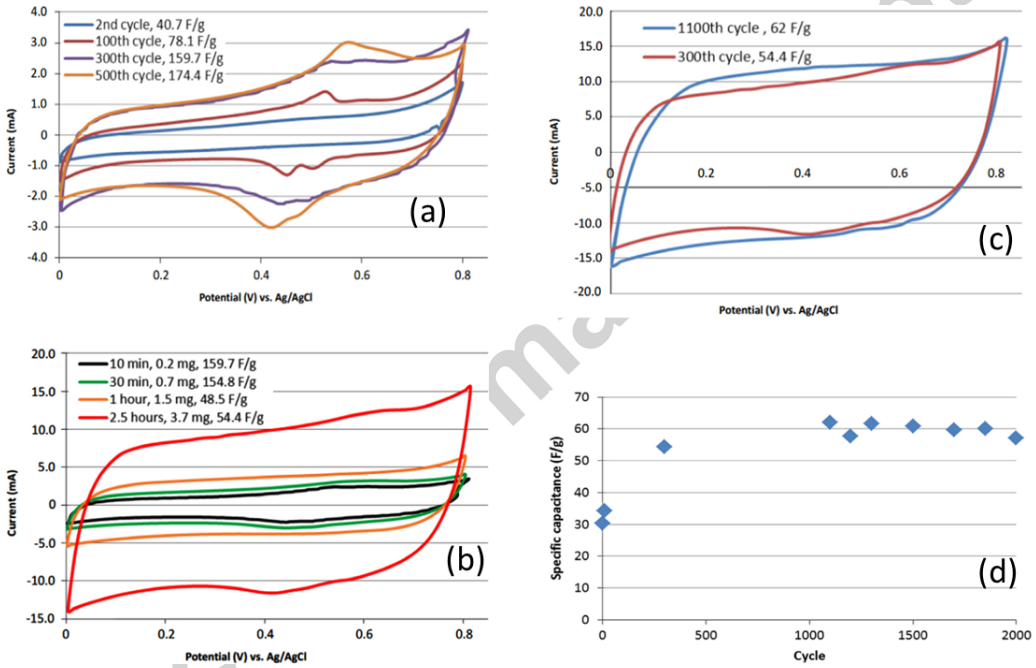

Fig. 29. (a) Voltammograms for a Mn_xO_y layer (0.2 mg/cm^2) deposited for 10 min. (b) 300th cycle voltammograms for layers deposited for different periods. (c) 300th and 1100th cycle voltammogram for a layer deposited for 2.5 h. (d) Evolution of specific capacitance of the layer deposited for 2.5 h during cycling. Reprinted with permission from Marsalek et al., 2015.

In another study forming MnO_2 via ESD (Dai et al., 2006), the hydrated MnO_2 film deposited at 230 ^{o}C from a $KMnO_4$ precursor solution is porous and cracked according to the SEM results. A specific capacitance of a thick deposited film was 149 F/g recorded at a scan rate of 500 mVs and 200 F/g at a scan rate of 5 mV/s, showing good cyclic performance. The initial specific capacitance was 163 F/g and showed a 103% of the initial specific capacitance, which could be retained after 10,000 cycles at a scan rate of 50 mV/s. Here too, the specific capacitance decreased from 267 to 135 F/g by increasing the load of active mass from 0.06 to 0.2 mg/cm^2.

3.3.4 VO_2/TiO_2 electrode materials

Binder-free electrodes of VO_2/TiO_2 nano-sponges, having easily tailored nano-architectures and composition, were synthesized by ESD (Hu et al., 2015). To form the metal oxide nano-architectures as layers, an ethanol solution of NH_4VO_3 and oxalic acid was made at 70 °C , and another ethanol solution of titanium(IV)isopropoxide with acetic acid. Combinations of both solutions were prepared referred to as VT1 (Ti/V=4), VT2 (Ti/V=2), and VT3 (Ti/V=1). To further dilute the solution, 40 ml 1, 2-propylene was added. Aluminum foils, nickel foams, and glass slides were used as substrates. ESD was done at a substrate temperature kept at 260 °C, with a distance between substrate and nozzle of 3cm. Residual carbonaceous substances were oxidised by annealing at 350 °C in air for 15 min followed by an thermal treatment at 500 °C under 5% NH_3/Ar atmosphere for 90 min. The obtained VO_2/TiO_2 nano-sponges (Fig. 30) showed an interconnected pore network and thereby a synergistic effect of the high capacity of VO_2 and the stability of TiO_2. The electrode exhibits a capacity of 86.2 mF/cm^2 (~548 F/g) and a cycleability with 84.3% retention after 1000 cycles (Fig. 30).

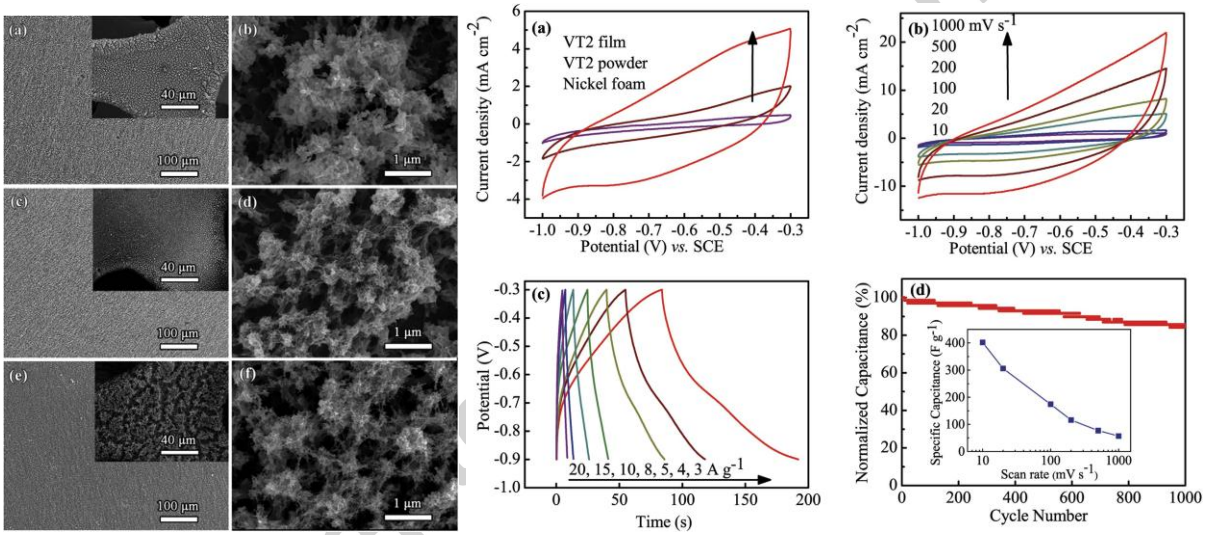

Fig. 30. Left panel: SEM images of VT films on Al-foil. (a,b) VT1, (c,d) VT2, and (e,f) VT3. The insets show films on Ni-foam. Right panel: Electrochemical performance of the VT2 film. CV curves for (a) the VT2 film, the VT2 powder and the Ni-foam (scan rate of 100 mV/s), and (b) the VT2 film at scan rates of 10, 20, 100, 200, 500, and 1000 mV/s. (c) Galvanoastatic charge-discharge curves of the VT2 film at current densities of 3, 4, 5, 8, 10, 15, and 20 A/g. (d) Cycling performance at a current density of 10 A/g over 1000 cycles - the inset shows the specific capacitance as a function of the scan rate. Reprinted with permission from Hu et al., 2015.

3.3.5 RuO_2 electrode materials

Ruthenium oxide thin films were fabricated by ESD with a precursor solution of $RuCl_3 \bullet xH_2O$ in a mixture of 80 vol % butyl carbitol and 20 vol % ethanol at a substrate temperature of 200°C (Fig. 31) (Kim et al., 2004). The electrochemical protonation may be the most responsible process for the redox reaction of anhydrous ruthenium oxide thin film, according to:

$$RuO_x(OH)_y + wH^+ + we^- \leftrightarrow RuO_{x-w}(OH)_{y+w}$$

The specific capacitance at a potential scan rate of 20 mV/s was 500 F/g and it decreased slightly with increasing potential scan rate up to 200 mV/s, also showing an excellent rate capability (Fig. 31).

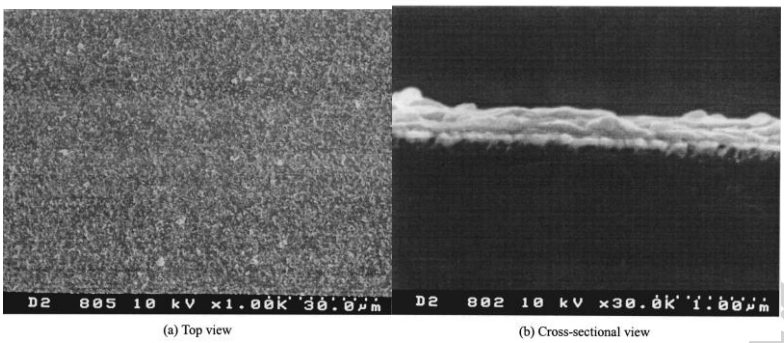

Fig. 31. SEM images of RuO_2 thin film prepared at 200°C: (a) Top view, and (b) cross-section view. Reprinted with permission from Kim et al., 2004.

Similar results were obtained by (Kim et al., 2001) using a one-step process ESD process to easily control the surface morphology. The as-prepared hydrated RuO_2 ($RuO_2 \bullet xH_2O$) thin films were amorphous, but become crystalline after annealing at temperatures > 200 ^{o}C. $RuO_2 \bullet xH_2O$ thin film electrode annealed at 200 ^{o}C showed a cyclic voltammogram indicative of a typical capacitive behaviour in 0.5 M H_2SO_4 electrolyte at a scan rate of 20 mV/s with an average specific capacitance of 650 F/g. The average specific capacitance was 640 F/g at 2 mV/s and 600 F/g at 50 mV/s, respectively, indicating that the average specific capacitance decreased only slightly with increasing scan rate (Fig. 32).

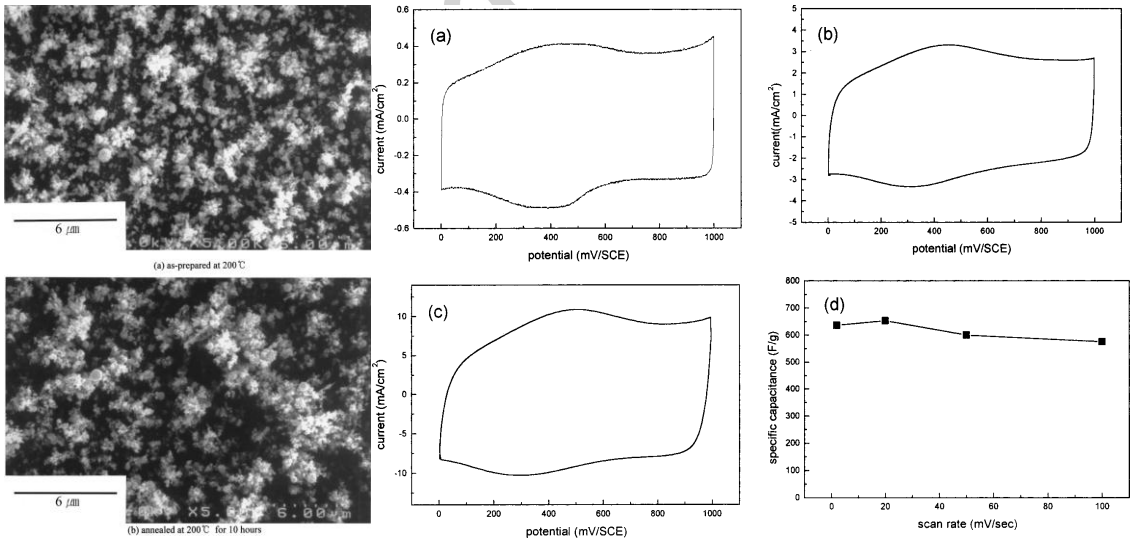

Fig. 32. Left panel: SEMs of ruthenium oxide thin film electrode for (a) as-prepared at 200°C and (b) Right panel: CVs of ruthenium oxide thin film electrode annealed at 200°C in 0.5 M H_2SO_4 at a scan rate of (a) 2 mV/s, (b) 20 mV/s, (c) 50 mV/s, (d) specific capacitance of ruthenium oxide thin film electrode at different scan rates. Reprinted with permission from Kim et al., 2001.

3.3.6 NiO@rGO electrode materials

A binder-free NiO@rGO composite supported on nickel foams was fabricated by ESD. A suspension of GO and nickel acetate was prepared in 1,2-propylene glycol (Zhang et al., 2015). A nickel foam substrate was heated to 250◦C, and the deposition was done with a flow rate of 3mL/h at 20 kV. Then, the black nickel foam was rinsed several times and dried in air afterwards. The loading mass was about 0.8mg/cm^2. The NiO nanoparticles were uniformly anchored onto the layered rGO sheets, thereby improving the electrolyte–electrode accessibility, allowing high electrochemical utilization of the NiO by maintaining open nano-channels of the composites (Fig. 33). This thus led to a high specific capacitance of 881 F/g at a current density of 0.5 A/g and about 75.7% of the capacitance was retained by increasing the current density to 50 A/g. Even after cycling for 3000 cycles at 20 A/g, 95% of the initial capacitance was delivered Fig. 33).

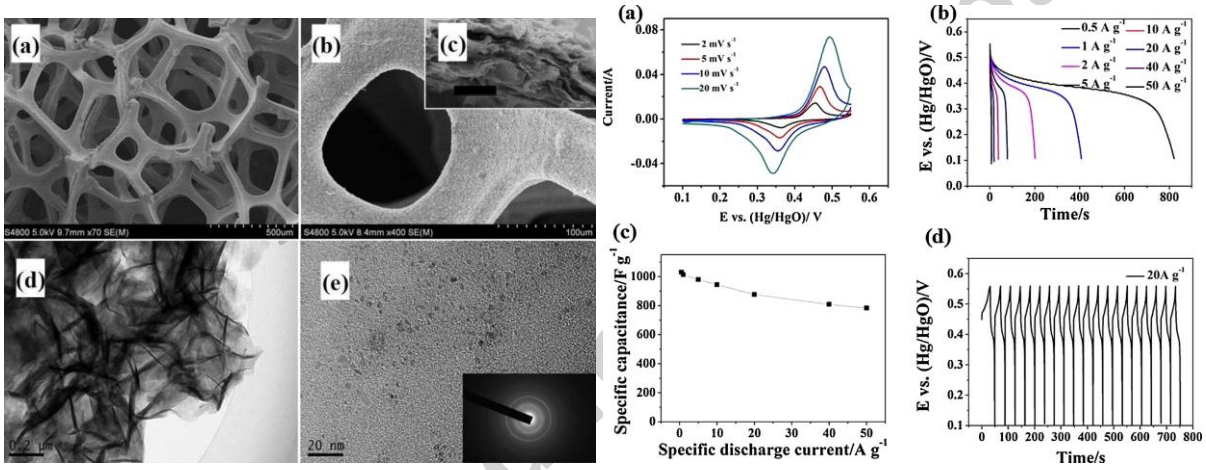

Fig. 33. Left panel: (a-b) SEM images, (c) cross-section SEM image, scale bar equals 600 nm, (d-e) TEM images and SAED pattern (inset) of the NiO@rGO composites. Right panel: (a) Cyclic voltammograms (b) Galvanostatic discharge curves of NiO@rGO composite films (c) Specific capacitances calculated from the discharge curves, (d) the galvanostatic charge-discharge curves at 20 A/g. Reprinted with permission from Zhang et al., 2015.

3.3.7 V_2O_5 electrode materials

In another study (Lee et al., 2017), polyacrylonitrile (PAN)/multi-walled carbon tube (MWNT) heteromat-mediated ultrahigh capacitance electrode sheets were used as an unusual electrode architecture. Here, vanadium pentoxide (V_2O_5) is applied as an electrode material to proof its feasibility. V_2O_5 electrode sheets are thus fabricated by a one-pot method via electrospraying (for V_2O_5 precursor/MWNT) and electrospinning (for PAN nanofiber) followed by calcination at 250 and 300 ^oC, so as to arrive at amorphous (V-250) or crystalline (V-300) V_2O_5 (Fig. 34).The heteromat V_2O_5 electrode sheets then offer 3D bicontinuous electron conduction pathways, facilitating the necessary redox reaction kinetics of V_2O_5. The electrochemical reaction in V_2O_5 electrodes can be expressed as follows:

$$V_2O_5 + xK^+ + xe^- \leftrightarrow K_xV_2O_5$$

wherein x is the mole fraction of reacted K^+ ions.

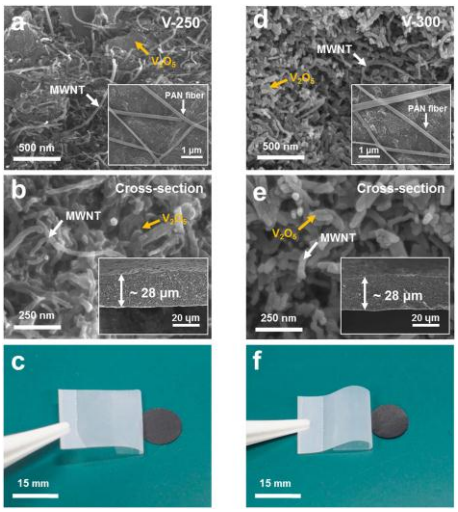

Fig. 34. Morphological characterization of V_2O_5 layers as defined in the text: (a-c) V-250 and (d-f) V-300 electrode sheets. (a,d) SEM surface images showing homogeneous dispersion of V_2O_5, MWNTs and PAN nanofibers – the insets are low-magnification photos. (b,e) SEM cros-section images. (c,f) An adhesion test using commercial 3M scotch® tape. Reprinted with permission from Lee et al., 2017.

Electrochemical data are collected in Fig. 35, where the caption explains the actual results. A substantially increase in the (electrode sheet-based) specific gravimetric electrode capacitances was obtained e.g. 134 $F/g_{electrode}$ compared to 29 $F/g_{electrode}$ for a reference V_2O_5 electrode, recorded at scan rate of 1 mV/s. Hence, the V_2O_5 electrode gave an significant increase of the specific energy/power densities as shown in the Ragone plot.

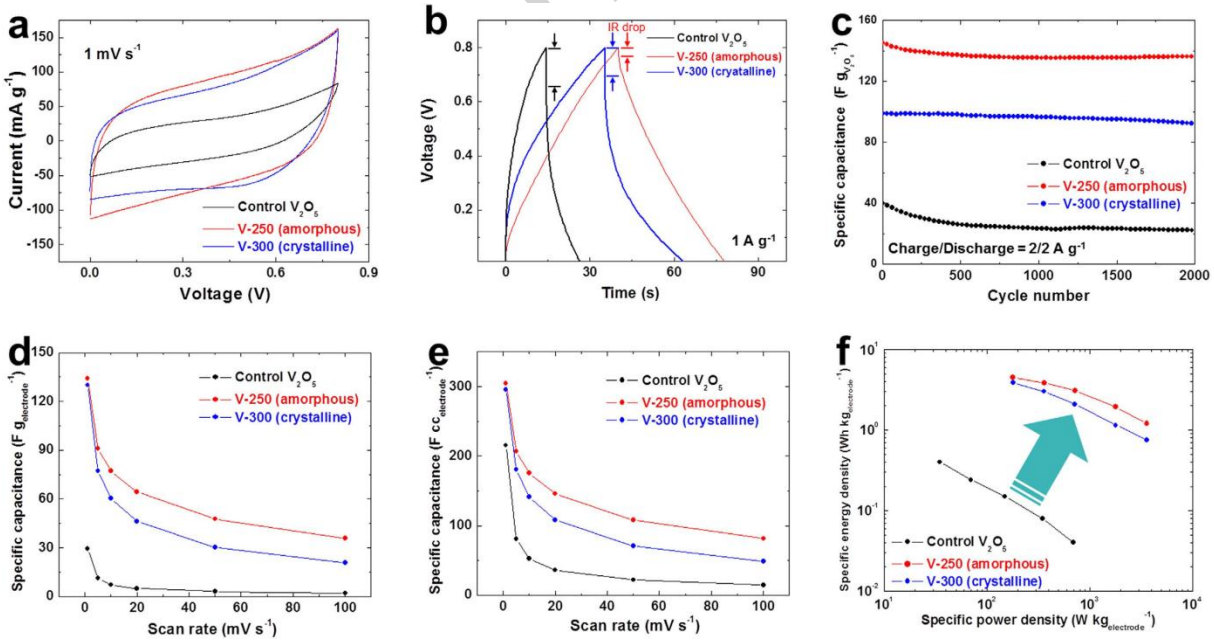

Fig. 35. Cyclic voltammetry curves showing typical Faradaic pseudocapacitive behaviour, measured at a scan rate of 1 mV/s (a), galvanostatic charge/discharge profiles measured at 1.0 A/cm^2 (b), comparison in cycling performance between the different electrodes measured at 2.0 A/g (c), comparison in the (electrode sheet-based) specific gravimetric capacitance (F/g) between the different electrodes vs scan rate (d), comparison in the (electrode based)

specific volumetric capacitance (F/cc) between the different electrodes vs scan rate (e), and a Ragone plot, with the cell weight taken as the electrode sheet weight only. Reprinted with permission from Lee et al., 2017.

4 ESD for Energy Conversion Devices (*(O)LEDSs and Quantum Dots*)

The new generation of light sources light emitting diodes (LEDs) and organic light-emitting diodes (OLEDs), including polymer light-emitting diodes (PLEDs) attracted considerable attention as used in solid lighting devices. (O)LEDs are more efficient than most traditional light sources due to their long lifetime, high reliability, and high efficiency, making these interesting in many applications. Besides, they seem to be environmental friendly, due to use of less toxic materials. Recently, the research has focused on new methods of fabricating flexible, low-cost electronic components and devices, other than the (O)LEDs, e.g. flexible displays, organics photovoltaics (OPV), organic thin film transistors (OTFT), etc.. Obviously, these products require mass and continuous production, such as the roll-to-roll (R2R) printing or coating. Among the employed techniques, non-contact coating methods, such as spray coating via, ESD and aerosol jet etc. are one of the most widely used. Only very recently, continuous and large area coating becomes available for future mass production (Kim et al., 2010). It remains however, important to realise that the surface roughness issue needs to be soughed out in order to arrive at a much more homogeneity in the layer thickness (Hwang et al., 2014).

4.1 ESD for LEDs

Today's LEDs have efficiencies around 20% where the remaining energy is converted into heat at the junctions of the LED modules (Shanmugan et al., 2014; Kuo et al., 1994; Lee et al., 2005). Unfortunately then, insufficient heat dissipation in LEDs, reduces the emission efficiency and also shortens a LED lifetime. Hence, thermal management is an important strategy to overcome these shortcomings. One of the solution is to form an isolation layer with very low thermal conductivity, which then gives a junction between the LED and metal Printed Circuit Board (PCB), providing a large thermal resistance, so the generated heat is rapidly transferred to a heat sink. Various ceramic interlayers showed improvements for the thermal conductivity of the base substrates and thus the performance of the device (Yin et al., 2013; Yang et al., 2014; Zheng et al., 2012; Figueroa et al., 2005). One of the solutions is an aluminium nitride (AlN) coating used for heat dissipation in the packaging of LEDs, since this material has a high optical transparency and is chemically and thermally stable (Zheng et al., 2012; Figueroa et al., 2005; Li et al., 2007; Rada & Triplett, 2010; Rada et al., 2008; Zuo et al., 2001; Shinde & Goela, 2006; Shen et al., 2015). However, as in many other new devices, cost reduction is an important requirement. Electrostatically sprayed AlN coatings, as a heat sink on Cu and Al substrates, provide the requirements for the electronics industry, as a highly conductive material with reasonable production costs (Jean et al., 2016). Applying these in a 1.2W LED at 700 mA, the effect of the thermal resistance (R_{ja}) and the thermal performance such as cooling are shown in Fig. 36. The figure shows the temperature distribution during operation for 60 minutes and after switching off the current. It was further observed that R_{ja} for the Cu is greater than that for the Al substrate, i.e. 16.2 ^{o}C/w and 15.1 ^{o}C/w, respectively. These results demonstrate that the temperature of the LED packages is significantly reduced if there is an AlN-coated Al substrate at a current of 700mA, fabricated via ESD (Fig. 36).

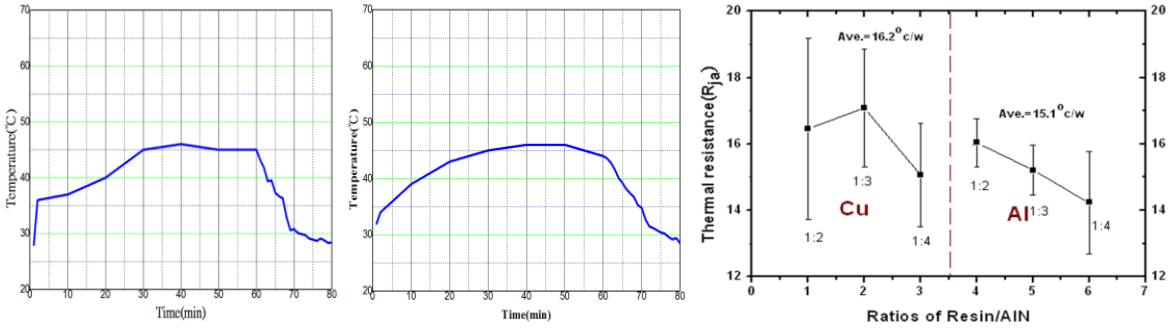

a b c

Fig. 36. Temperature profiles of an AlN coated Cu (a) and an Al (b) substrate, measured during applying a 700mA current and after switching it off after 60 mins. A comparison of (R_{ja}) for a 1.2W LED on AlN-coated Cu and Al substrates (c). Reprinted with permission from Jean et al., 2016.

4.2 ESD for OLEDs

(O)LEDs have attracted enormous interest, because they are light and flexible compared to more state-of-the-art inorganic electroluminescence (EL) materials used in the LEDs. Typically, there are two fabrication methods of thin-film OLEDs, e.g. vacuum deposition of low-molecular-weight organics, and casting polymer materials from solution, where the low-molecular-weight organic ELs are made via vacuum deposition, and the polymer-type OLEDs are then manufactured via casting. It however needs to mention that polymer materials are usually difficult to evaporate, making fabrication of a multi-layered structure complicated when using low-molecular-weight organics. Also, the solvents used for layer-to-layer deposition affects the interfaces by mutual dissolution. Therefore, ESD is an interesting alternative with great potential, where even patterning can be done. This patterning was carried out with a dichlorobenzene (DCB) solvent to form an Emissive layer (EML)) on top of an ITO glass (Lee et al., 2015). Here, the distance between the quartz nozzle with a 211µm diameter and the substrate was 50 to 100 µm. The line patterning width was controlled by the distance between the nozzle and the substrate, under the cone-jet mode as shown in Fig. 37. Hence, the results proved that inkjet printing via ESD is a versatile method for optimal patterning to draw very narrow lines, with a jetting fluid diameter of only 15 µm, even after drying.

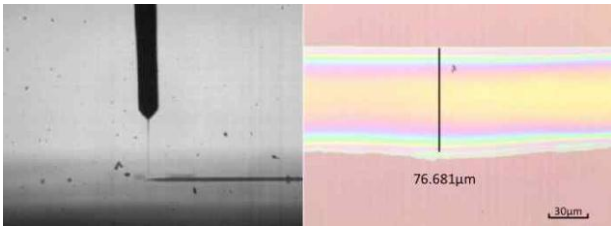

a b

Fig. 37. Results of the patterning with dichlorobenzene solvent, an outside nozzle diameter of 211µm, and a Jet thickness of 15µm; the ejection from the nozzle (a) and the patterned line (b). Reprinted with permission from Lee et al., 2015.

ESD was also used to deposit an organic layer for polymer organic light-emitting diode devices (Hwang et al., 2012). The electrospray was used to produce nanometer-scale thin films via micro-sized droplets. PLED were thus made using a blended solution of either poly(N-vinyl carbazole) (PVK), 2-(4-biphenylyl)-5-(4-tertbutylphenyl)-1,3,4-oxadiazole (PBD), N,N'diphenyl-N,N'-Bis(3-methylphenyl)-[1,1-biphenyl]-4,4'-diamine (TPD), and tris(2-(4-tolyl) phenylpyridine) iridium ($Ir(mppy)_3$) dissolved in chlorobenzene (CB), DCB, or a mixture of CB and 1,2-DCB. Two inks were applied as shown in Table 2 and Table 3.

Table 2. Ratio of the PLED ink – data taken from Hwang et al., 2012.

	Ink 1*	**Ink 2***
Poly(N-vinyl carbazole (PVK)	61	41.5
2-(4-biphenylyl)-5-(4-tert-butylphenyl)-1,3,4-oxadiazole (PBD)	24	41.5
N,N'diphenyl-N,N'-bis(3-methylphenyl)-[1,1-biphenyl]-4,4'-diamine (TPD)	9	14.8
tris(2-(4-tolyl)phenylpyridine)iridium ($Ir(mppy)_3$)	6	4.2

** Each value refers to weight percentage of material in solution.*

The difference between Ink1 and 2 is the ratio of hole and electron transport materials.

Table 3. Summary of device performances – data taken from Hwang et al., 2012.

Process	**Ink**	**Solvent**	**EML (nm)**	**Cd/A (max)**	**Lm/W (max)**
Spin coating	Ink1	CB	78	24	10.0
ESD	Ink1	CB/DCB (5:3)	100	15	6.0
ESD	Ink1	CB/DCB (5:3)	120	18	6.6
ESD	Ink2	CB/DCB (5:3)	70	18	7.5
ESD	Ink2	CB/DCB (5:3)	100	24	9.2
ESD	Ink2	CB/DCB (1:1)	103	23	8.6

EML: emissive layer; CB: chlorobenzene; DCB: dichlorobenzene

Fig. 38 shows that a 70-150 nm thick light-emitting organic layers was formed with about 1 nm surface roughness. The photoluminescence (PL) at 407 nm was observed using electrosprayed poly(N-vinyl carbazole) films, whereas a peak at 410 nm was observed with the spin-coated ones. Similar difference in peak position was observed between aromatic and nonaromatic solvents in the spin-coating process.

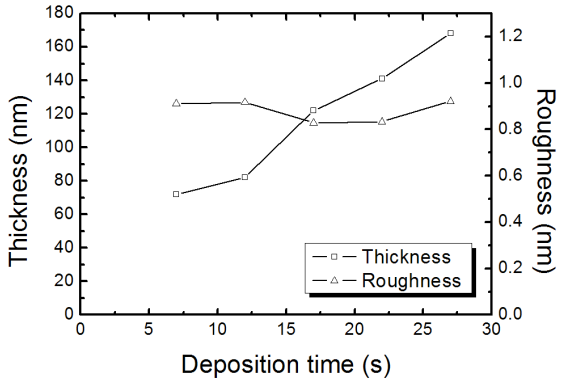

Fig. 38. PVK film thickness and roughness as a function of deposition time. Reprinted with permission from Ref. Hwang et al., 2012.

PLED devices were manufactured with a ratio of PVK/PBD/TPD/Ir(mppy)=61:24:9:6 (ink 1) for both the spin-coating and electrospray processes. With respect to the solvents, CB works best for the spin-coating process and DCB for the electrospray process. In Fig. 39, the current-voltage characteristics of the PVK film using different solvents and processing methods is shown. Samples with similar thickness, fabricated with aromatic solvents (mixtures of chlorobenzene, CB and dichlorobenzene, DCB) showed a higher current density than those fabricated with a nonaromatic solvent (1, 2-dichloroethane, DCE). Also the PVK film made by electrospray showed a lower current density than that of spin-coated ones. Besides, these results proof that the PVK thin films were affected by the processing method and the molecular structure of the solvent as shown Fig. 39. Hence, it is possible to fabricate layers by electrospray with similar properties as with spin-coating by adjusting the solvent, i.e. they showed maximum current efficiency of 24 Cd/A, which is comparable with that of the spin-coating process.

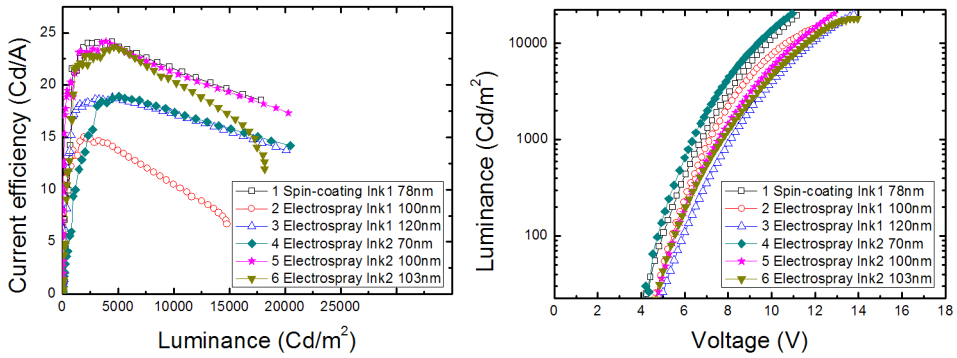

Fig. 39. Device performance made by spin-coating and ESD. The thicknesses of the EMLs are given in the insets. Reprinted with permission from Hwang et al., 2012.

In another study (Anzai et al., 2012), ESD was applied for manufacturing an overlayer on a thin film made via spin-coating so as to form a laminate structure. Unfortunately, the ESD process is not suitable for stacking various layers without any mixing effect (Fig. 40).

In this study, the emitted droplet size was minimized by the use of adding acetone to the solution. Two different polymer materials were used for the fabrication of the multi-layered structure. The first one was poly[2-methoxy-5-(2ethylhexyloxy)-1,4-phenylenevinylene] (MEH-

PPV) and the second one was poly[2,5-di(hexyloxy)cyanoterephthalylidene] (CN-PPV), but each of the materials was dissolved in an o-dichlorobenzene (o-DCB) solvent at a 0.6 and 0.4 wt%, respectively. PEDOT:PSS was then used to equalise and homogenise the indium tin oxide (ITO) glass substrate. The middle panel of Fig. 40 displays optical micrographs of the MEH-PPV film surface at various ratios of the original solution to acetone, showing the impact of the acetone. The nozzle to substrate distance was 8 cm, and the spray time was taken 1 h. The spectra in Fig. 41 were obtained from various mixed films of MEH-PPV and CN-PPV prepared by either successive spin coating or ESD. It turns out that for the ESD deposited films the mixed films of MEH-PPV and CN-PPV are clear linear combinations in contrast to the spin-coated samples. This obviously made clear that the double-layer structure is in place.

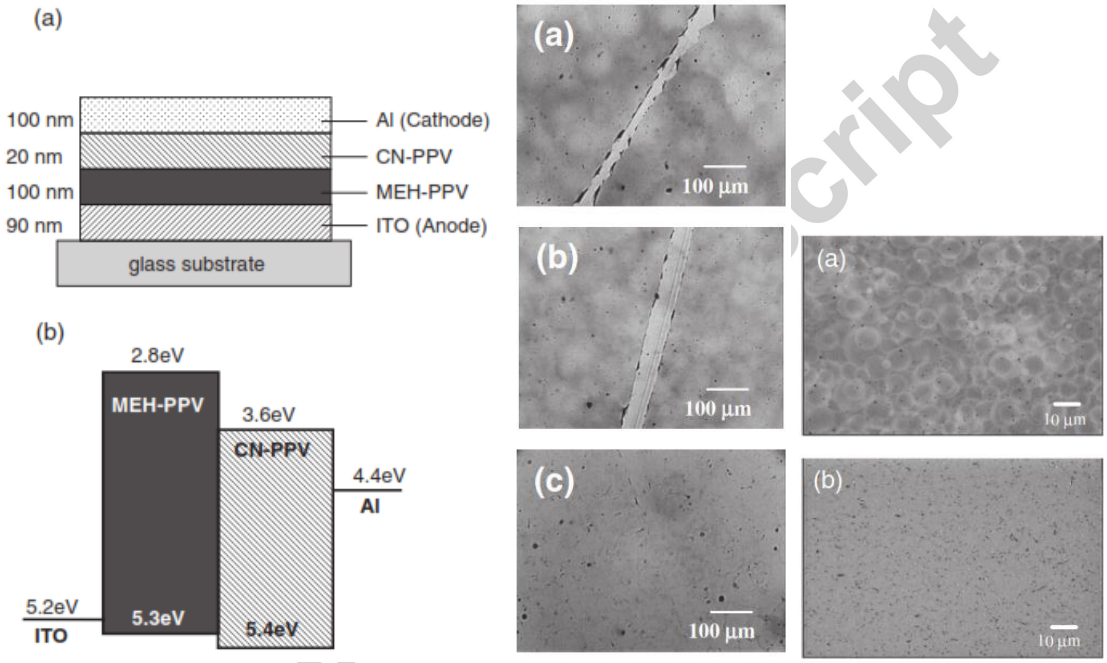

Fig. 40. Left panel: (a) Target multi-layered OLED structure and (b) energy diagram. Middle panel: Micrographs of MEH-PPV film surface formed by ESD. The ratios of MEH-PPV in o-DCB at 0.6 wt % to acetone were (a) 2:1, (b) 1:2, and (c) 1:5. The center line in (a) and (b) are scratches marked for thickness measurements. Right panel: Micrographs of MEH-PPV surfaces formed by ESD with nozzle inner diameters of 100 mm (a) and 30 mm (b). Reprinted with permission from Anzai et al., 2012.

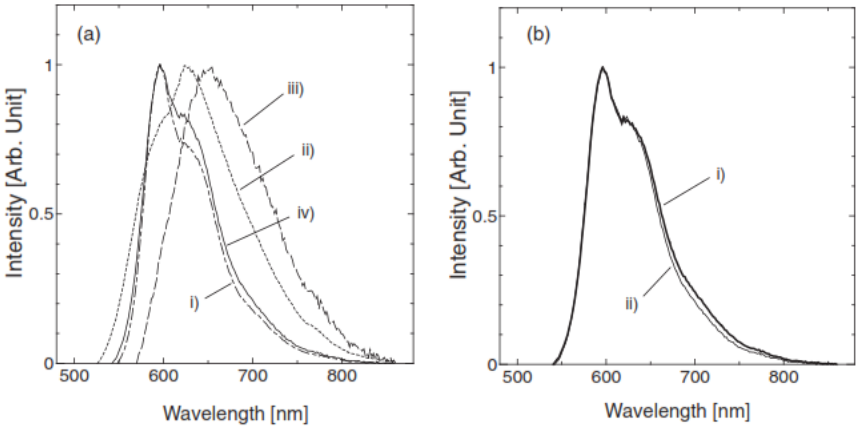

Fig. 41. (a) Fluorescence spectra of MEH-PPV (i), CN-PPV (ii), mixture of MEH-PPV and CN-PPV via spin-coating (iii), and CN-P Quantum DotsPV/MEH-PPV double layer formed by ESD (iv). (b) Spectra obtained from linear combination of CN-PPV and MEH-PPV (i) and spectra with a ratio of 1:4 and CN-PPV/MEH-PPV double layer (ii). Reprinted with permission from Anzai et al., 2012.

4.3 Quantum Dots

Lumenescent properties can also be achieved by introducing Quantum Dots (QDs) in chalcogenide glass films, where e.g. the QD-doped glass layer then serves as a compact, on-chip light source for planar photonic devices (Li et al., 2017). ESD in that respect is a versatile method form these layers as typically, well established methods as spin coating lead to excessive material waste, show little control on the pattern of the film and has difficulties in scaling-up. Here the concentration of the QDs in the ESD-solvent was chosen to ensure one or none QD is present per liquid droplet. The transmission electron microscopy images of the films proof QD dispersion with reduced 10 nm gold NPs and 5 nm QDs aggregations (Fig. 42). This dispersion is attributed to the isolation of an individual QD in one droplet and the way the solvent has been vaporised during the time of flight. Photoluminescence spectra of the films of chalcogenide glass doped with QDs reveals similar emission results as reported by the manufacturer.

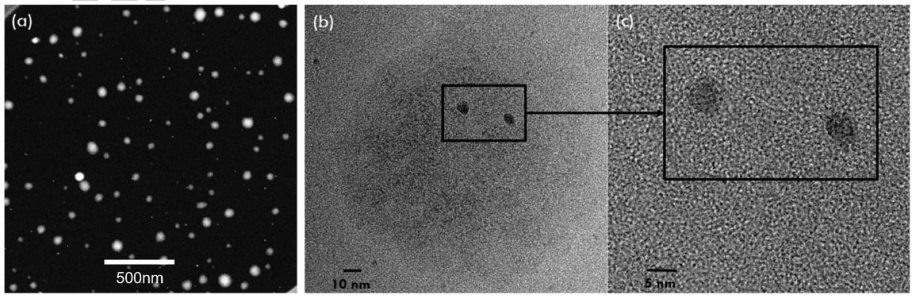

Fig. 42. TEM images of gold NPs doped $Ge_{23}Sb_7S_{70}$ made by ESD. (a) Dispersion of $Ge_{23}Sb_7S_{70}$ droplets; (b) evidence of a ~100 nm diameter droplet containing two gold NPs; (c) higher magnification showing NP size of nominally 5–10 nm. Reprinted with permission from Li et al., 2017.

Green-red (GR) and blue-red (BR) bilayer stacked quantum dots (QDs) were made via ESD, in a for large-scale, high throughput, uniform thin film fabrication system without using any annealing process (Yin et al., 2017). The morphology of the thin film is controlled by varying the flow rate, voltage (3.5 to 4.5kV), distance between the substrate and electrode (~4cm) and the deposition time (20s). Here then, appropriate QDs were dispersed in solvents (hexane:octane=4:1) and sprayed onto 1cm^2 quartz collectors, so as to form a layer by layer stack. Nevertheless, for the mixed samples, equimolar B (or G) and R QDs were suspended in the solvents in advance., and those were sprayed for 40 s. The photo-behaviour of these QDs was analysed with several techniques and the observed results are then ascribed to the energy transfer between different visible QDs (heterotransfer), and were estimated as 0.57 ± 0.01 and 0.65 ± 0.02 ns for GR and BR systems, respectively, which agree well with theoretical calculations. It was further shown that with respect to their geometrical proximity, the mixed QD layers with GR and BR had qualitatively higher heterotransfer efficiencies of 64% and 81%, compared to stacked QD layers, with efficiencies of 23% and 64%, respectively.

In another study (Ho et al., 2014) it was shown that QDs for LED fabrication using ESD leading to nanoscale thin QD-layers (25 nm) and smooth surfaces (roughness ~3.16 nm) has significant benefits including simple and flexible control, low cost, large-scale processability, and compatibility for multiple-layer-structure devices such as QD-LEDs. These layers were formed by a mixture of two aliphatic liquids as solvent (hexane:octane=4:1). The ZnO nanoparticles were dispersed in ethanol (Fig. 43). The QD-LED demonstrated a maximum luminance of 23 000 cd/m^2 (see Fig. 43), a maximum current efficiency of ~6.0 cd/A, and a FWHM of about 35 nm. Hence, ESD proved to a promising process for the fabrication of multiple-layer-structured devices for a direct and nearly dry patterning for commercial production, as compared to the spin-coating process, where CB and DCB solvents cannot be used since they dissolve the underlying organic hole transport layers. Hence, it confirms the strength of ESD where these solvent can be easily employed, with minimal damage of the underlying organic layers.

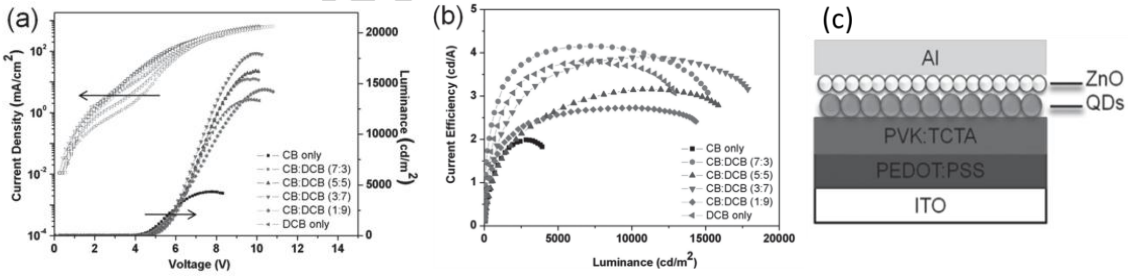

Fig. 43. ElectroLumenescence characteristics of QD-LEDs obtained with CB, DCB and the CB:DCB mixtures as solvents: a) I–V–L characteristics and b) current efficiency of the QD-LEDs fabricated by ESD, and (c) QD-LED device structure (ITO/PEDOT:PSS/(PVK:TCTA) (20 wt%)/QDs/ZnO/Al) Reprinted with permission from Ho et al., 2014.

5 Conclusions

In this review it was shown that electrohydrodynamic atomization (EHDA) or electrospraying stands out in thin film deposition (ESD) in different areas, such as solar cells, photoelectrochemical cells, rechargeable batteries, capacitors, and (O)LEDs as well as for the formation of layers for using quantum dots. Since charge transfer of either electrons or ions is

an important issue for electrodes in those devices, the morphology of it, is of utmost importance, because it will reflects the exchange area for these charge carriers. Obviously, with ESD, several morphologies were achieved to suit the various requirements, so as to mention: flat, rough (porous), and reticular structures. Furthermore, the method of ESD is flexible as it allows non- or poor volatile precursors to use once dissolved in solution – provided the solvent is able to be atomised. This then opens up the possibility to form materials with complex compositions as is often seen in today's devices with improved performance.

References

Abbas T.A., Slewa L.H., Khizir H.A. and Kakil S.A., (2017), Synthesis of cobalt oxide (Co_3O_4) thin films by electrostatic spray pyrolysis technique (ESP), *J. Mater Sci: Mater Electron., 28, 1951-1957.*

Abernathy C., Bates Jr. C., Anani A., Haba B. and Smestad G., (1984), Production of single phase chalcopyrite $CuInSe_2$ by spray pyrolysis, *Appl. Phys. Lett., 45, 890.*

Agostinho L.L.F., (2013), Electrohydrodynamic Atomization in the Simple-Jet Mode Out-scaling and Application. PhD thesis ISBN 978-90-6464-635-5, Delft University of Technology, Delft, The Netherlands.

Ahn S., Kim C., Yun J.H., Gwak J., Jeong S., Ryu B.-H. and Yoon K., (2010), $CuInSe_2$ (CIS) Thin Film Solar Cells by Direct Coating and Selenization of Solution Precursors, *J. Phys. Chem. C, 114, 8108-8113.*

Ali M., Abbas M., Shah S.K., Tuerhong R., Generosi A., Paci, B., Hirsch L. and Gunnella R., (2012), Realization of solution processed multi-layer bulk heterojunction organic solar cells by electro-spray deposition, *Org. Electron., 13, 2130–2137.*

Altamura G., Wang M., Choy K-L., (2015), Improving efficiency of electrostatic spray-assisted vapor deposited $Cu_2ZnSn(S,Se)_4$ solar cells by modification of Mo/absorber interface, *Thin Solid Films, 597, 19–24.*

Anzai H., Watanabe Y. and Sakamoto, T., (2012), *Jap. J. Appl. Phys., 51, 6S.*

Barrows A. T., Pearson A. J., Kwak C. K., Dunbar A. D. F., Buckley A. R. and Lidzey D. G., (2014), *Energy Environ. Sci., 7, 2944–2950*.

Beidaghi M. and Wang C., (2012), Micro-Supercapacitors Based on Interdigital Electrodes of Reduced Graphene Oxide and Carbon Nanotube Composites with Ultrahigh Power Handling Performance. *Adv. Funct. Mater., 22: 4501–4510.*

Beidaghi M., Wang Z.F., Gu L. and Wang C.L., (2012), Electrostatic spray deposition of graphene nanoplatelets for high-power thin-film supercapacitor electrodes ,*J Solid State Electrochem, 16, 3341.*

Bodnár E., Grifoll J., Rosell-Llompart J., (2018), Polymer solution electrospraying: A tool for engineering particles and films with controlled morphology*, J. Aerosol Science, present issue, pp to be filled*

Bougnot J., Duchemin S. and Savelli M., Chemical spray pyrolysis of $CuInSe_2$ thin films, (1986), *Solar Cells, 16, 221.*

Burschka J., Pellet N., Moon S. J., Humphry-Baker R., Gao P., Nazeeruddin M. K. and Gratzel M., (2013), *Nature, 499, 316–319*.

Cao F. and Prakash J., (2002), A comparative electrochemical study of $LiMn_2O_4$ spinel thin-film and porous laminate, *Electrochimica Acta, 47, 1607-1613.*

Castillo J., Martin S., Rodriguez-Perez D., Higuera F. and Garcia-Ybarra P., (2018), Nanostructured porous coatings via electrospray atomization and deposition of nanoparticle suspensions*, J. Aerosol Science, present issue, pp to be filled*

Chandrasekhar P.S., Kumar N., Swami S.K., Dutta V. and Komarala V.K., (2016), Fabrication of perovskite films using an electrostatic assisted spray technique: the effect of the electric field on morphology, crystallinity and solar cell performance, *Nanoscale, 8, 6792-6800*

Chen C.H., Buysman A.A.J., Kelder E.M. and Schoonman J., (1995), Fabrication of $LiCoO_2$ thin film cathodes for rechargeable lithium battery by electrostatic spray pyrolysis, *Solid State Ionics, 80, 1-4.*

Chen C., Put P.J.J.M. Van Der and Schoonman J., (1996), Morphology control of thin LiCoO,. *J. Mat. Chem.*, *6(5), 765–771*.

Chen C.H., Kelder E.M., Jak M.J.G. and Schoonman J., Electrostatic spray deposition of thin layers of cathode materials for lithium battery, (1996), *Solid State Ionics, 86-88, 1301-1306*.

Cho S.H., Hwang S.W., Kim B.H., Bae K.Y. and Yoon W.Y., (2016). Electrochemical properties of Li metal batteries with P (PEGMA)-coated lithium trivanadate cathode and Li power anode, *J. Nanosci. Nanotechn., 16*(10), *10607-10612*.

Chung K.Y., Shu D. and Kim K.B., (2004), Determination of the potential range responsible for the replacement of surface film on LiMn2O4. *Electrochimica Acta*, *49*(6*), 887-898.*

Chung K.Y., Ryu C.-W. and Kim K.-B., (2005), Onset Mechanism of Jahn-Teller Distortion in 4 V $LiMn_2O_4$ and Its Suppression by

$LiM_{0.05}Mn_{1.95}O_4$ (M=Co, Ni) Coating, *J. Electrochem. Soc.*, *152*, *A791*.

Dai, Y., Wan, K., Zhao J. and Xie J., (2006), Manganese oxide film electrodes prepared by electrostatic spray deposition for electrochemical capacitors from the $KMnO_4$ solution, *J. Power Sources, 161(1), 737-742*.

Damien D., Anjusree G.S., Sreekumaran Nair A. and Shaijumon M.M., (2016), TiO_2 fibre/particle nanohybrids as efficient anodes for lithium-ion batteries, *RSC Adv.*, *6(51), 45802–45808.*

Dhanabalan A., Li X., Agrawal R., Chen C. and Wang C., (2013), Fabrication and Characterization of SnO_2/Graphene Composites as High Capacity Anodes for Li-Ion Batteries, *Nanomaterials*, *3*(4), *606-614.*

Docampo P., Hanusch F., Stranks S. D., Doblinger M., Feckl J. M., Ehrensperger M., Minar N. K., Johnston M. B., Snaith H. J. and Bein T., (2014), *Adv. Energy Mater., 4, 140035*.

Dokko K., Anzue N., Mohamedi M., Itoh T. and Uchida I., (2004), Raman spectro-electrochemistry of $LiCo_xMn_2$-xO_4 thin film electrodes for 5 V lithium batteries, *Electrochemistry Communications*, *6(4), 384-388.*

Eberspacher C., Fredric C., Pauls J. and Serra K., (2001), Thin-film CIS alloy PV materials fabricated using non-vacuum, particles-based techniques, *Thin Solid Films, 387, 18-22.*

Figueroa U., Salas O. and Oseguera J., (2005), Deposition of AlN on Al substrates by reactive magnetron sputtering, *Surf. Coat. Techn., 200, 1768-1776.*

Fujimoto M., Kado T., Takashima W., Kaneto K. and Hayase S., (2006), Dye-sensitized solar cells fabricated by electrospray coating using tio2 nanocrystal dispersion solution, *J. Electrochem. Soc., 153, A826.*

Fujimoto M., Kado T., Takashima W., Kaneto K. and Hayase S., (2006), Dye-sensitized solar cells fabricated by electrospray coating using TiO_2 nanocrystal dispersion solution, *J. Electrochem. Soc. 153(5), A826-829.*

Fujimoto K., Onoda K. and Ito S., (2007), Exploration of layered-type pseudo four-component Li-Ni-Co-Ti oxides. *Applied Surface Science*, *254*(3), *704-708.*

Fujimoto K., Onoda K., and Ito S., (2007). High-Throughput Preparation and Characterization of Powder and Thin-Film Library for Electrode Materials, *Materials Science Forum*, *534-536*, *469-472*.

Fujimoto K., Ikezawa K. and Ito S., (2011), Charge–discharge properties of a layered-type $Li(Ni,Co,Ti)O_2$ powder library, *Sci. Techn. Adv. Mat.*, *12*(5), *54203.*

Fukuda T. Takagi K., Asano T., Honda Z., Kamata N., Ueno K., Shirai H., Ju J., Yamagata Y. and Tajima Y., (2011), Bulk heterojunction organic photovoltaic cell fabricated by the electrospray deposition method using mixed organic solvent, *Phys. Status Solidi, RRL5, 229-231*.

Fukuda T., Takagi K., Asano T., Honda Z., Kamata N., Shirai H., Ju J., Yamagata Y. and Tajima I.Y., (2012), Improved power conversion efficiency of organic photovoltaic cell fabricated by electrospray deposition method by mixing different solvents, *Jap. J. Appl. Phys., 51, 1-5.*

Fukuda T., Toda A., Takahira K., Suzuki K., Liao Y., Hirahara M., Saito M. and Osaka I.,(2016), Molecular ordering of spin-coated and electrosprayed P3HT:PCBM thin films and their applications to photovoltaic cell, *Thin Solid Films, 612, 373–380.*

Fukuda T., Toda A., Takahira K., Kuzuhara D. and Yoshimoto N., (2017), Improved performance of organic photovoltaic cells with PTB7-Th: PC71 BM by optimized solvent evaporation time in electrospray deposition, *Organic Electronics, 48, 96-105*.

Ganan-Calvo A., Lopez-Herrera J., Herrada M, Ramos A., Montanero J. M., (2018), Review on the physcis of electrospray: from electrokinetics to the operating conditions of Taylor cone-jets, and beyond, *J. Aerosol Science, present issue, pp to be filled*

García-Tamayo,E., Valvo,M., Lafont,U., Locati,C., Munao,D. and Kelder E.M., (2011). Nanostructured Fe_2O_3 and CuO composite electrodes for Li ion batteries synthesized and deposited in one step, *J. Power Sources*, *196(15), 6425-6432.*

Ho M.D., Kim N., Kim D., Cho S.M. and Chae H. (2014), CdSe/ZnS Quantum Dot Thin Film Formation by an Electrospray Deposition Process for Light-Emitting Devices. *Small, 10, 4142-4146.*

Hu C.C., Xu H., Liu X., Zou F., Qie L., Huang Y. and Hu X., (2015), VO_2/TiO_2 Nanosponges as Binder-Free Electrodes for High Performance Supercapacitors, *Sci. Rep., 5, 16012.*

Hu G., Deng X., Peng Z., Du K., Cao Y., Liu Z. and Xiao Z. (2008), Co/Mn-Coated $LiNiO_2$ Cathode Materials by Solid-State Reaction at Room Temperature. *Rare Metal Mat. Eng.*, *37(11), 1881-1886*.

Hu H., Wang D., Zhou Y., Zhang J., Lv S., Pang S., Chen X., Liu Z., Padture N. P. and Cui G., (2014), *RSC Adv., 4, 28964–28967*.

Hwang J.K., Bae S. and Kim D.S., (2014), A development and evaluation of micro-gravure coater for printed electronics, *Jap. J. Appl. Phys., 53, 5S3*.

Hwang W., Xin G. Cho M., Cho S.M. and Chae H., (2012), Electrospray deposition of polymer thin films for organic light-emitting diodes, *Nanoscale Res. Lett***.**, *7,52*.

Jaworek A. and Sobczyk A.T., (2008), Electrospraying route to nanotechnology: An overview, *Journal of Electrostatics, 66, 197-219.*

Jaworek A., Sobczyk A.T., Krupa A., Lackowski M. and Czech T., (2009), Electrostatic deposition of nanothin films on metal substrate, *Bull. Pol. Ac. Sc. Tech. Sc., 57, 1.*

Jaworek A., Sobczyk A. T. and Krupa A., (2018), Electrospray application to powder production and surface coating, *J. Aerosol Science, present issue, pp to be filled*

Jean M.-D., Jiang J.-B, Xu M.-S and Chien J.-Y., (2016), Using AlN-coated heat sink to improve the heat dissipation of LED packages, *MATEC Web of Conf., 71, 04005*.

Jeon N. J., Noh J. H., Kim Y. C., Yang W. S., Ryu S. and Seok S. I., (2014), *Nat. Mater., 13, 897–903*.

Jeon N.J., Lee H.G., Kim Y.C., Seo J., Noh J.H., Lee J. and Seok S.I. (2014), , *J. Am. Chem. Soc., 136, 7837–7840.*

Jeon N. J., Noh J. H., Yang W. S., Kim Y. C., Ryu S., Seo J. and Seok S. I., (2015), *Nature, 517, 476–480*.

Kim I.-H. and Kim K.-B.,(2001), Ruthenium Oxide Thin Film Electrodes for Supercapacitors, *Solid State Lett., 4(5), A62-A64*.

Kim I.-H. and Kim K.-B., (2004), Ruthenium oxide thin film electrodes prepared by electrostatic spray deposition and their charge storage mechanism, *J. Electrochem. Soc., 151, E7-E13*.

Kim J.H., Nam K.W., Ma S.B. and Kim K.B., (2006), Fabrication and electrochemical properties of carbon nanotube film electrodes, *Carbon, 44(10), 1963-1968.*

Kim J-S., .Chung W.-S., Kim K., Kim D.Y., Paeng K.J., .Jo S.M. and Jang S.Y., (2010), Performance optimization of polymer solar cells using electrostatically sprayed photoactive layers, *Adv. Funct. Mater., 20, 3538-3546.*

Kim J.S., Choi K.H., Kim K.D., Kim C.H., Bae S.W. and Kim D.S., (2010), An application of ESD technology for the R2R printing process, *J Mech Sci Technol, 24, 301*.

Kim Y., Kim G., Lee J., Lee K., (2012), Morphology controlled bulk-heterojunction layers of fully electro-spray coated organic solar cells, *Sol. En. Mater. Sol. Cells, 105, 272-279*.

Kim Y., Lee L., Kang H. Kim G., Kim N. and Lee, K., (2012), Controlled electro-spray deposition of highly conductive PEDOT: PSS films, *Sol. Energy Mater. Sol. Cells, 9, 39-45.*

Koike S., and Tatsumi K., (2007), Preparation and performances of highly porous layered $LiCoO_2$ films for lithium batteries, *J. Power Sources, 174(2), 976-980*.

Krishna K. V., Dutta V. and Paulson P. D., (2003), Effect of electric field on spray deposited CdTe thin films, *Thin Solid Films, 444,17–22*.

Kuo P.K.G, Auner W. and Wu Z.L., (1994), Microstructure and thermal conductivity of epitaxial AlN thin films, *Thin Solid Films, 253, 223-227.*

Lafont U., Anastasopol A., Garcia-Tamayo E. and Kelder E.M., (2012), Electrostatic spray pyrolysis of $LiNi_{0.5}Mn_{1.5}O_4$ films for 3D Li-ion microbatteries, *Thin Solid Films*, *520(9), 3464-3471*.

Largeot C., Portet C., Chmiola J., Taberna P., Gogotsi Y. and Simon P., (2008), Relation between the ion size and pore size for an electric double-layer capacitor, *J. Am. Chem. Soc., 30, 2730*.

Lee J., Liang K., An K. and Lee Y., (2005), Nickel oxide/carbon nanotubes nanocomposite for electrochemical capacitance, *Synth. Met., 150, 153.*

Lee J.H., Kim J.A., Kim J-M, Lee S-Y, Yeon S-H and Lee, S.-Y, (2017), Beyong slurry-cast supercapacitor electrodes: PAN/MWNT heteromat-mediated ultrahigh capacitance electrode sheets, *Scient. Rpts, 7, 41708.*

Lee J. W., Cuomo J.J., Cho Y.S. and Keusseyan R.L., (2005), Aluminum Nitride Thin Films on an LTCC Substrate, *J. Amer. Ceram. Soc., 88(7), 1977-1980.*

Lee S.H., Nguyen X.H., Gim Y. and Ko S.K., (2015), Study on electrohydrodynamic jetting performance of organic solvents, *J Mech Sci Technol., 29, 4767.*

Lee T., Cho K., Oh J. and Shin D., (2007), Fabrication of $LiCoO_2$ cathode powder for thin film battery by aerosol flame deposition, *Journal of Power Sources, 174, 394-399*.

Lee W., Seol D.J., Cho A.N. and Park N.G., (2014), High-Efficiency Perovskite Solar Cells Based on the Black Polymorph of $HC(NH_2)_2PbI_3$,*Adv. Mater., 26, 4991–4998*.

Li C., Novak S., Denisov S.A., McClenaghan N.D., Patel N., Agarwal A., Richardson K, and Deng W.W., (2017), Electrospray deposition of quantum dot-doped $Ge_{23}Sb_7S_{70}$ chalcogenide glass films, *Thin Solid Films, 626, 194-199.*

Li F., Jiao Y., Xie S. and Li J., (2015), Sponge-like porous TiO_2/ZnO nanodonuts for high efficiency dye-sensitized solar cells, *J. Power Sources, 280, 373-378.*

Li X., Ren Z.A. and Sun D.Q., (2007), An investigation of nitrided layer prepared by direct current nitrogen arc discharge. *Mat. Sci. Engin. A, 443, 219-223.*

Li X. and Wang C., (2013), Engineering nanostructured anodes via electrostatic spray deposition for high performance lithium

ion battery application, *J. Mater. Chem. A*, *1(2), 165–182.*

Liu M. Z., Johnston M. B. and Snaith H. J., (2013), *Nature, 501, 395–398*.

Mao S., Wen Z.H., Kim H.J., Lu G.H., Hurkey P. and Chen J.H., (2012), A general approach to one-pot fabrication of crumpled graphene-based nanohybrids for energy applications, *ACS nano., 6, 7505.*

Marsalek J., Chmelar J., Pocedic J. and Kosek J., (2015), Morphological and electrochemical study of Mn_xO_y nanoparticle layers prepared by electrospraying, *Chem. Engin. Science, 123, 292-299.*

Milliron D., Mitzi D., Copel M. and Murray C., (2006), Solution-processed metal chalcogenide films for p-type transistors, *Chem. Mater., 18, 587-590*.

Mitzi D., Kosbar L., Murray C., Copel M. and Afzali A., (2004), High-mobility ultrathin semiconducting films prepared by spin coating, *Nature, 428, 299*.

Mitzi D., Copel M., Murray C., (2006), High-Mobility p-Type Transistor Based on a Spin-Coated Metal Telluride Semiconductor, *Adv. Mater., 18, 2448*.

Mitzi D., Yuan M., Liu W., Kellock A., Chey S., Deline V. and Schrott A., (2008), A High-Efficiency Solution-Deposited Thin-Film Photovoltaic Device, *Adv. Mater., 20, 3657*.

Mitzi D., Yuan M., Liu W., Kellock A., Chey S., Gignac L. and Schrott A., (2009), Hydrazine-based deposition route for device-quality CIGS films, *Thin Solid Films, 517, 2158-2162*.

Mohamedi M., Makino M., Dokko K., Itoh T. and Uchida I., (2002), Electrochemical investigation of $LiNi_{0.5}Mn_{1.5}O_4$ thin film intercalation electrodes, *Electrochimica Acta*, *48, 79-84.*

Mohamedi M., Takahashi D., Itoh T. and Uchida I., (2002), Electrochemical stability of thin film $LiMn_2O_4$ cathode in organic electrolyte solutions with different compositions at 55° C, *ElectroChim. Acta, 47, 3483-3489*.

Mohamedi, M., Takahashi D., Itoh T., Umeda M. and Uchida I., (2002), ESD Fabricated Thin Films of Spinel $LiMn_2O_4$ for Lithium Microbatteries: I. Effects of Thickness. *J. Electrochem. Soc.*, *149(1), A19*.

Mooney J. and Radding S., Spray pyrolysis processing, (1982), *Annu. Rev. Mater. Sci., 12, 81.*

Neagu R., Djurado E., Ortega L. and Pagnier T., (2006), ZrO_2-based thin films synthesized by electrostatic spray deposition: Effect of post-deposition thermal treatments, *Solid State Ionics, 177, 1443-1449.*

Nie W., Tsai H., Asadpour R., Blancon J. Ch., Neukirch A. J., Gupta G., Crochet J. J., Chhowalla M., Tretiak S., Alam M. A., Wang H. L. and Mohite A. D., (2015), *Science, 347, 6221–6224*.

Nishizawa M., Uchiyama T., Dokko K., Yamada K., Matsue T. and Uchida I., (1998), Electrochemical Studies of Spinel $LiMn_2O_4$ Films Prepared by Electrostatic Spray Deposition,. *Bull. Chemical Soc. Jap., 71(8), 2011-2015*.

Niu S., Lv W., Zhou G., Shi H., Qin X., Zheng C., Zhou T., Luo C., Deng Y., Li B., Kang F. and Yang Q. H., (2016), Electrostatic-spraying an ultrathin, multifunctional and compact coating onto a cathode for a long-life and high-rate lithium-sulfur battery, *Nano Energy, 30, 138-145*.

Panthani M.G., Akhavan V., Goodfellow B., Schmidtke J.P., Dunn L., Dodabalapur A., Barbara P.F. and Korgel B.A., (2008), Synthesis of $CuInS_2$, $CuInSe_2$, and $Cu(In_xGa_{1-x})Se_2$ (CIGS) Nanocrystal "Inks" for Printable Photovoltaics, *J. Am. Chem. Soc.*, *130, 16770.*

Park S.E., Hwang J.Y., Kim K., Jung B., Kim W. and Hwang J., (2011), Spray deposition of electrohydrodynamically atomized polymer mixture for active layer fabrication in organic photovoltaics, *Sol. En. Mater. Sol. Cells, 95, 352-356*.

Pognon G., Brousse T., Demarconnay L. and Belanger D., (2011), Performance and stability of electrochemical capacitor based on anthraquinone modified activated carbon, *J. Power Sources., 196, 4117*.

Qu B.H., Chen Y.J., Zhang M., Hu L.L, Lei D.N., Lu B.A., Li Q.H., Wang Y.G., Chen L.B. and Wang T.H., (2012), Cobalt sulfide nanoparticles decorated graphene composite electrodes for high capacity and power supercapacitors, *Nanoscale, 4, 7810.*

Rada N. Triplett G. Graham S. and Kovaleski. S., (2008), High-speed thermal analysis of high power diode arrays, *Solid State Electronics., 52, 10.*

Rada N.M. and Triplett G.E., (2010), Thermal and spectral analysis of self-heating effects in high-power LEDs, *Solid State Electronics., 54, 4.*

Raja Ram P., Thangaraj R. and Agnihotri O.P., Thin film CdZnS/$CuInSe_2$ solar cells by spray pyrolysis, (1986), *Bull. Mater. Sci.*, *8, 279*.

Ramesh M., Boopathi K. M., Huang T. Y., Huang Y. C., Tsao C. S. and Chu C. W., (2015), *ACS Appl. Mater. Interfaces, 7, 2359–2366.*

Roncallo S., Painter J.D., Cousins M., Lane D. and Rogers K., (2008), A method to quantify the degree of uniformity of thickness of thin films, *Thin Solid Films, 516, 8493-8497*.

Rosell-Llompart J, Grifoll J. and Loscertales I., (2018), Electrosprays in the cone-jet mode: from Taylor cone formation to spray development*, J. Aerosol Science, present issue, pp to be filled*

Scheideler W.J. and Chen C-H., (2014), The minimum flow rate scaling of Taylor cone-jets issued from a nozzle, *Appl. Phys. Lett., 104, 024103*

Shanmugan S., Mutharasu D.A. and Haslan H. (2014), A study on AlN thin film as thermal interface material for high power LED, *Int. J. Electron. Comput. Sci. Eng., 2(1), 296-300*

Shay J., Wagner S. and Kasper H., (1975), Efficient $CuInSe_2$/CdS solar cells, *Appl. Phys. Lett., 27, 89.*

Shen W.Q., Zhu Y.W. and Wang G.L., (2015), Luminescent properties of $Sr_4Si_3O_8Cl_4:Eu^{2+}$, Bi^{3+} phosphors for near UV InGaN-based light-emitting-diodes, *Appl. Sci., 5., 1494-1502*

Shinde S.L. and Goela J. (Eds.), (2006), High Thermal Conductivity Materials*, Springer, New York, ISBN 978-0-387-22021-5.*

Shirakata S., Murakami T., Kariya T. and Isomura S., Preparation of CuInSe2 thin films by chemical spray pyrolysis, (1996), *Jap. J. Appl. Phys., 35, 191.*

Shu D., Yoon K., Il W. and Kim K., (2003), Electrochemical investigations on electrostatic spray deposited $LiMn_2O_4$ flms, *Journal of Power Sources*, *114*, *0-10.*

Shui J.L., Jiang G.S., Xie S. and Chen C.H., (2004), Thin films of lithium manganese oxide spinel as cathode materials for secondary lithium batteries, *Electrochimica Acta, 49, 2209-2213*

Shui J.L., Yu Y., Yang X.F. and Chen C.H., (2006), $LiCoPO_4$-based ternary composite thin-film electrode for lithium secondary battery. *Electrochem. Comm.*, *8(7), 1087-1091*.

Sun Y., Zhang L., Wang S., Lieberwirth I., Yu Y. and Chen C. (2013), Walnut-like vanadium oxide film with high rate performance as a cathode material for rechargeable lithium batteries, *Journal of Power Sources, 228, 7-13.*

Tomar M. and Garcia F., (1982), A ZnO/p-CuInSe2 thin film solar cell prepared entirely by spray pyrolysis, *Thin Solid Films, 90, 419-423*.

van Zomeren A.A., Kelder E.M., Marijnissen J.C.M. and Schoonman J., (1994), The production of thin films of LiMn2O4 by electrospraying, *J. Aerosol Sci., 25, 6, 1229-1235.*

Wang H., Casalongue H.S., Liang Y. and Dai H.J., (2010), $Ni(OH)_2$ Nanoplates Grown on Graphene as Advanced Electrochemical Pseudocapacitor, *J. Am.Chem.Soc., 132, 7472.*

Wang M., Sun Y., Chen H., Zhang Y., Wu X., Huang K. and Feng S., (2017), Enhanced photoelectrochemical activity of nanostructured $ZnFe_2O_4$ thin films prepared by the electrospray technique, *Cryst. Eng. Comm., 19, 772–775*.

Wu J., Chen C., Hao Y. and Wang C., (2015), Enhanced electrochemical performance of nanosheet ZnO/reduced graphene oxide composites as anode for lithium-ion batteries, *Colloids and Surfaces A: Physicochem. Eng. Asp.*, *468, 17-21.*

Wu J., Qin X., Zhang H., He Y.B., Li B., Ke L. and Kang F., (2015), Multilayered silicon embedded porous carbon/graphene hybrid film as a high performance anode. *Carbon*, *84(1), 434-443.*

Wu J.B., Li Z.G, and Lin Y., (2011), Porous NiO/Ag composite film for electrochemical capacitor application, *Electrochim. Acta, 56, 2116.*

Xiao Z., Bi C., Shao Y., Dong Q., Wang Q., Yuan Y., Wang C., Gao Y. and Huang J., (2014), *Energy Environ. Sci., 7, 2619–2623*.

Yang K.S, Chung C.H., Tu C.W., Wong C.C., Yang T.Y. and Lee M.T., (2014), Thermal spreading resistance characteristics of a high power light emitting diode module, *Appl. Thermal Engin., 70(1), 361-368.*

Yin S., Tseng K.J. and Zhao .J., (2013), Design of AIN-based micro-channel heat sink in direct bond copper for power electronics, *Appl. Thermal Engin., 52(1), 120-129*.

Yin W., Kim N., Jeong J., Kim K.S., Chae H. and Ahn T.K., (2017), Efficient Heterotransfer between Visible Quantum Dots, *J. Phys. Chem. C*, *121(9), 4799–4805.*

Yoon H, Woo J.H, Joshi B., Ra Y.M., Yoon S.S., Kim H.Y., Ahn S.J. Yun J.H., Gwak, J., Yoon, K.H., and James, S.C., (2012), $CuInSe_2$ (CIS) Thin Film Solar Cells by Electrostatic Spray Deposition, *J. Electrochem. Soc., 159(4), H444-H449.*

Yoon H., Na S.H., Choi J.H., Kim M.W., Kim H., An H.S., Min B.K., Ahn SJ, Yun J.H., Gwak J., Yoon K.H., Kolekar S.S., van Hest M.F.A.M., Al-Deyab S.S., Swihart M.T. and Yoon S.S., (2014), Carbon- and Oxygen-Free $Cu(InGa)(SSe)_2$ Solar Cell with a 4.63% Conversion Efficiency by Electrostatic Spray Deposition, *Appl. Mater. Interfaces, 6, 8369−8377.*

Yoon H., Kim M.W., Kim H., Al-Dey S.S., James S.C., Ahn S. and Yoon S.S., (2015), Three dimensional web-like fibrous $CuInS_2$ film, *Appl. Surf. Sci., 351, 588–593.*

Yoon W., Ban S., Lee K., Kim K., Kim M. G., and Lee J. M., (2001), Electrochemical characterization of layered LiCoO2 films prepared by electrostatic spray deposition, *J. Power Sources, 97-98, 282-286.*

Yoon W.S., Chung K.Y., Oh K.H. and Kim K.B., (2003), Changes in electronic structure of the electrochemically Li-ion

deintercalated $LiMn_2O_4$ system investigated by soft X-ray absorption spectroscopy, *Journal of Power Sources, 119-121, 706-709*.

Youn H.C., Bak S.M., Park S.H., Yoon S.B, Roh K.C. and Kim K.B., (2014), One-step preparation of reduced graphene oxide/carbon nanotube hybrid thin film by electrostatic spray deposition for supercapacitor applications, *Met. Mater. Int., 20, 975-981.*

Yu, T., Lin, B., Li, Q., Wang, X., Qu, W., Zhang, S. and Deng, C., (2016), First exploration of freestanding and flexible $Na_{2+2}Fe_{2-x}(SO_4)$@porous carbon nanofiber hybrid films with superior sodium intercalation for sodium ion batteries, *Phys.Chem.Chem.Phys., 18, 26933*.

Yu Y., Shui J.L., Jin Y. and Chen C.H., (2006), Electrochemical performance of nano-SiO2 modified $LiCoO_2$ thin films fabricated by electrostatic spray deposition (ESD). *Electrochim. Acta*, *51*(16*), 3292-3296.*

Yurteri C.U., Hartman R.P.A. and Marijnissen J.C.M., (2010), Producing Pharmaceutical Particles via Electrospraying with an Emphasis on Nano and Nano Structured Particles - A Review, *KONA Powder and Particle Journal, 28, 91-115*

Zangmeister C.D., (2010), Preparation and Evaluation of Graphite Oxide Reduced at 220^{o}C, *Chem. Mater., 22, 5625.*

Zhang H., Gua D., Zhu,J., Li Q., Chen L. and Wang T., (2015), A layer-by-layer deposition strategy of fabricating NiO@ rGO composites for advanced electrochemical capacitors, *Electrochim. Acta, 152, 378-382.*

Zhang, M., Lei D.N., Yin X.M., Chen L.B., Li Q.H., Wang Y.G. and Wang T.H., (2010), Fast synthesis of SnO_2/graphene composites by reducing graphene oxide with stannous ions, *J. Mater. Chem., 20, 5538.*

Zhao X.Y, Wang X., Lim S.W., Qi D., Wang R., Gao Z.Q., Mi B.X., Chen Z.-K., Huang W. and Deng W.W., (2014), Enhancement of the performance of organic solar cells by electrospray deposition with optimal solvent system, *Sol. Energy Mater. Sol. Cells, 121, 119-125*.

Zheng X., Ren Z., Li, X. and Wang Y., (2012), Microstructural characterization and mechanical properties of nitrided layers on aluminum substrate prepared by nitrogen arc, *Appl. Surf. Sci., 259, 508-514.*

Zhou H., Chen Qi., Li G., Luo S., Song T. B., Duan H. S., Hong Z., You J., Liu Y. and Yang Y., (2014), *Science, 345, 542–546*.

Zuo Z.J., North M.T. and Wert K.L., (2001), High heat flux heat pipe mechanism for cooling of electronics, *IEEE Trans. Comp. Pack. Techn., 24(2), 220-225.*

Zhu C., Kopold P., van Aken P.A., Maier J., and Yu Y., (2016), High Power-High Energy Sodium Battery Based on Threefold Interpenetrating Network, *Adv. Mater, 28, 2409-2416.*

Highlights

- Electrostatic Spray Deposition (ESD) stands out in thin film deposition.
- ESD allows to control thin layer morphologies.
- ESD is a powerful tool in materials synthesis.
- ESD is used to improve energy devices such as batteries, PECs, (O)LEDS, and capacitors.